Current methods for characterising mixing and flow in microchannels

Joelle Aubin, Montse Ferrando, Vladimir Jiricny

Current methods for characterising mixing and flow in microchannels

Joëlle Aubin [a,b,*], Montse Ferrando [c], Vladimir Jiricny [d]

[a] Université de Toulouse, INP, LGC (Laboratoire de Génie Chimique), 4 allée Emile Monso BP-84234, 31432 Toulouse Cedex 4, France
[b] CNRS, LGC, 31432 Toulouse Cedex 4, France
[c] Department of Chemical Engineering, ETSEQ, University Rovira I Virgili, Tarragona, Spain
[d] Department of Separation Processes, Institute of Chemical Process Fundamentals, Prague, Czech Republic

A B S T R A C T

This article reviews existing methods for the characterisation of mixing and flow in microchannels, micromixers and microreactors. In particular, it analyses the current experimental techniques and methods available for characterising mixing and the associated phenomena in single and multiphase flow. The review shows that the majority of the experimental techniques used for characterising mixing and two-phase flow in microchannels employ optical methods, which require optical access to the flow, or off-line measurements. Indeed visual measurements are very important for the fundamental understanding of the physics of these flows and the rapid advances in optical measurement techniques, like confocal scanning laser microscopy and high resolution stereo micro particle image velocimetry, are now making full field data retrieval possible. However, integration of microchannel devices in industrial processes will require on-line measurements for process control that do not necessarily rely on optical techniques. Developments are being made in the areas of non-intrusive sensors, magnetic resonance techniques, ultrasonic spectroscopy and on-line flow through measurement cells. The advances made in these areas will certainly be of increasing interest in the future as microchannels are more frequently employed in continuous flow equipment for industrial applications.

1. Introduction

Due to the vast application field of micromixers and micro-structured mixers, such as homogenisation, chemical reaction, dispersion and emulsification, the efficiency of mixing in these devices is very important for the overall process performance. Indeed, mixing will affect various process parameters including heat and mass transfer rates, process operating time, cost and safety, as well as product quality. For this reason, it is important to understand the mixing process occurring in micromixers; to do this one must to be able to characterise and evaluate the mixing performance and the outcomes of the mixing process.

Several definitions of mixing exist in the field of chemical engineering. Danckwerts (1952) discussed the differences between complete segregation and perfect mixing in the context of reactor design, particularly for binary mixtures of liquids, and defined the intensity of segregation, which is the most cited measure of mixing. Later, Fournier et al. (1996), Baldyga and Bourne (1999) introduced the concepts of macro-, meso- and micro-mixing. More recently, Kukukova et al. (2009) have proposed an alternate approach, which defines segregation or mixing as being composed of three separate dimensions (the intensity of segregation, the scale of segregation and the rate of change of segregation), each existing at three scales of observation (the macro or equipment size scale, the meso scale and the micro scale being the scale at which the smallest phenomena occur). The generic framework of this approach allows for the characterisation of both single and multiphase mixing applications through concentration homogeneity, and length and time scales. This generalised definition of mixing defined by Kukukova et al. (2009) covers the well known definitions of mixing and also introduces new components, which have never explicitly been identified.

In the case of single phase applications in microchannels, mixing is largely controlled by molecular diffusion due to the predominantly laminar flow present in microchannels. In the scale of dimensions considered here, i.e. channel widths/depths ranging from a few hundred micrometers to a few millimeters, the mixing process by molecular diffusion is extremely slow, since the mixing time is proportional to d_l^2/D, where d_l is the characteristic diffusional path (typically the channel width) and D is the molecular diffusivity. Extremely slow mixing is especially true for liquids, which have small diffusivities. Thus, in order to mix effectively at this scale in a reasonable time, fluids must be

* Corresponding author at: Laboratoire de Génie Chimique, 4 allée Emile Monso BP-84234, 31432 Toulouse Cedex 4, France. Tel.: +33 5 34 32 37 14; fax: +331 5 34 36 97.
E-mail address: joelle.aubincano@ensiacet.fr (J. Aubin).

manipulated so that the interfacial surface area between the fluids is increased massively and the diffusional path is decreased, thereby decreasing the time required to complete the mixing process. Various mechanisms for contacting and mixing fluids exist, including hydrodynamic focusing, manifold splitting and recombination, T- and Y-junctions, chaotic mixing (Ehrfeld et al., 2000; Hessel et al., 2005). Therefore, in order to effectively design microchannels for mixing operations, a methodology that enables the mixing performance to be evaluated is required.

For gas–liquid and liquid–liquid mixing applications, the performance of the mixing operation is typically judged by the characteristics of the dispersion generated. These characteristics may include the physical properties of the dispersion, such as droplet or bubble size and size distribution, and also the hydrodynamics of the flow. Both the physical properties of the dispersion and the hydrodynamics are particularly important for mass transport and reaction applications since interfacial area and local hydrodynamics are key parameters, but also for product engineering applications where highly controlled physical properties are of key importance for the quality of the desired product.

Currently, a number of methodologies are employed for characterising the performance of various kinds of mixing operations in micro devices. Both experimental and numerical techniques exist, each of them having their advantages and limitations.

Modelling the mixing phenomena by simulation methods (e.g. computational fluid dynamics, lattice-Bolzmann method) is an attractive option, since it provides local three-dimensional flow information, which may be difficult or even impossible to access with experimental techniques. As a result, there are a large number of computational studies of mixing in single phase flow micro devices, and an increasing number of applications to gas–liquid and liquid–liquid dispersions. Although modelling laminar flow in micro devices reduces the difficulties related to turbulent flow modelling, which are often encountered in macro scale reactors, it introduces a number of new physical and computational difficulties related to surface effects (including surface roughness, wall slip, wettability and surface tension) and numerical solution accuracy (Fletcher et al., 2009). As a result, there is a continual need for experimental methodologies for mixing characterisation, which will not only help validate and develop the numerical techniques but also enable performance verification in industrial applications. The numerical methodologies for characterising mixing will not be detailed further here, as this review focuses on experimental characterisation methods only.

Understanding the characteristics of the flow, mixing and the outcomes of the mixing process in micro devices through accurate experimental measurements is very important for the design of these devices and their consequent integration in multi scale processes. A number of experimental techniques and methodologies have been specifically developed for the characterisation of mixing in micro devices; others are based on well established methods for the study of mixing operations in macro scale reactors, which have been modified for micro scale applications.

In this paper, the objective is to review and analyse the currently existing experimental methods used for characterising the performance of single phase liquid mixing and the outcomes of mixing gas–liquid and liquid–liquid flows in micro devices. For each characterisation method, the principle, the resulting information, the device requirements, the limitations, as well as some examples are detailed. In addition, for illustrative purposes, some example results have been taken from the literature. The type of information presented has been chosen such that this review may act as a guide for selecting an appropriate methodology that is adapted to the device, application and the type of required information. In addition, it should further enable the identification of mixing characteristics that are not attainable by the reported currently available experimental methods, giving direction to further developments in this area.

2. Single phase liquid mixing

2.1. Mixing quality

Mixing quality in miniaturised devices can be characterised using a number of different approaches, giving qualitative and/or quantitative information on the homogeneity of concentration and the length scales of the mixing system. This section details the principal methods used for characterising mixing in microchannel devices. In addition to the comprehensive information given in the following paragraphs, Table 1 summarizes the main requirements, limitations and associated difficulties of each technique.

2.1.1. Dilution-based characterisation methods

The principle of these methods relies on contacting a dye-containing liquid stream with a transparent, uncoloured liquid stream in a transparent device (or a device equipped with a viewing window). The spreading of the dye is visualised and monitored along the micro device using a microscope coupled with an imaging technique (video camera or high-speed camera). Mixing is judged complete when the concentration of the dye is uniform across the channel cross section. This method provides qualitative information on the intensity of segregation or the homogeneity of concentration that can be used to compare different devices or operating conditions within the same series of experiments. In a more quantitative manner, an approximate mixing time may also be deduced by determining the length required for visually-complete mixing. There are two principal limitations of this technique. The first is that the microchannel or the zone of interest in the device must be made of optically transparent material. Secondly, visualisation of the mixing process is conducted perpendicular to the direction of the flow. Consequently, images provide information that is averaged over the depth of the microchannel. This means that the difference between a perfectly mixed system and a multi-layered system (whereby the fluid lamellae are bent or arranged horizontally) cannot be distinguished, as will be pointed out in some examples below.

2.1.1.1. Dilution of coloured dyes. Due to the relatively simple experimental set-up, there are a number of studies reported in the literature (see for example: Hessel et al. (2003); Wong et al. (2004); Schönfeld et al. (2004); Lee et al. (2006)) that characterize mixing in micromixers via the visualisation of coloured dyes. Fig. 1 shows some examples of these studies and the type of information that can be obtained using this characterisation method. In these examples, concentrated solutions of blue dye, which provides excellent contrast, are contacted with colourless pure water in multilamination, T- and split-and recombine micromixers, respectively. In the multilamination and the split-and-recombine mixers (Figs. 1(a) and (c)) studied by Hessel et al. (2003) and Schönfeld et al. (2004), the different coloured fluid lamellae are arranged more or less side-by-side with no vertical superposition. The mixing quality and flow structures can clearly be observed at different positions along the mixer. Fig. 1(b) shows the mixing of dyes in a T-micromixer presented by Wong et al. (2004) at Reynolds numbers where flow instabilities and vortices occur. In this case, the different fluid lamellae are no

Table 1
Summary of resulting information, requirements and limitations of current experimental methods for characterising mixing.

Characterisation method	Resulting information	Micro device requirements	Advantages/limitations/associated difficulties	Selected examples
Dilution of coloured dyes	Qualitative information on mixing quality Indirect approximation of mixing time	Transparent device or device with transparent viewing window	Visualisation of the mixing process is conducted perpendicular to the direction of the flow. Consequently the information obtained is spatially averaged over the depth of the micromixer. This makes it difficult to distinguish perfectly mixed systems and complex multi-layered mixing patterns, and may result in the measurement of *overly* short mixing times. Appropriate for mixing in single and two phase systems	Hessel et al. (2003), Schönfeld et al. (2004), Wong et al. (2004), Lee et al. (2006)
Dilution of fluorescent species	Qualitative information on mixing quality Indirect approximation of mixing time 3D concentration maps possible	Transparent device or device with transparent viewing window	Using conventional microscopy, the resulting information is averaged over the depth of the device. Associated with confocal scanning microscopy, which enables point-wise measurement of the fluorescent dye through the depth of the micro device, 3-dimensional concentration data throughout the mixer can be retrieved. Appropriate for mixing in single and two phase systems	Knight et al. (1998), Johnson et al. (2002), Stroock et al. (2002), Hoffmann et al. (2006)
Acid–base or pH indicator reactions	Qualitative information on mixing quality Indirect approximation of mixing time	Transparent device or device with transparent viewing window	Visualisation of the mixing process is conducted perpendicular to the direction of the flow. Consequently, no information on the spatial mixing quality through the depth of the device is obtained. Results depend on the acid/base concentration ratios used Predominantly used for mixing in single phase systems	Branebjerg et al. (1995), Schwesinger et al. (1996), Liu et al. (2000), Kim et al. (2004), Cha et al. (2006), Kockmann et al. (2006), Lee et al. (2006),
Reactions yielding coloured species	Qualitative information on mixing quality Indirect approximation of mixing time	Transparent device or device with transparent viewing window	The coloured product appears only when the reagents are sufficiently mixed. This avoids the measurement of *overly* short mixing times with complex multi-layered mixing patterns that is inherent to most of the other visualisation techniques. Some reactions may form a solid product, which limits their use for characterising micromixers. Predominantly used for mixing in single phase systems	Mensinger et al. (1995), Hessel et al. (2003), Hardt et al. (2006)
Competing parallel reactions	Quantitative information on the yield of the secondary reaction. The greater the yield of the secondary product, the poorer the micromixing quality. No direct information on mixing time is accessible; however, mixing time may be deduced indirectly from the concentration measurements	For off-line measurements, there are no particular requirements For on-line measurements using UV–Vis spectroscopy, the measurement cell or the micromixer must transparent	For off-line measurements, long time delays between sampling from the mixer and sample analysis may promote (in certain configurations) the secondary reaction if mixing is not complete in the device. For the Villermaux/Dushman reaction, the amount of secondary product (iodine) formed depends strongly on the pH of the reacting solution. The acid concentration employed must be adapted to the flow rates used such that the iodine measurements are sensitive enough to distinguish different mixing performances. It is imperative that the same reaction conditions are used in order to relatively compare different mixing devices. Predominantly used for mixing in single phase systems	Ehrfeld et al. (1999), Ehlers et al. (2000), Panic et al. (2004), Keoschkerjan et al. (2004), Nagasawa et al. (2005), Aoki and Mae (2006), Kockmann et al. (2006)
Monitoring species concentration	1-dimensional profiles or 2-dimensional maps of species concentration, depending on the measurement technique used Both types of information allow the characteristic scale of fluid lamellae in the device to be identified, which can be related to mixing time	For photometric, fluorescence and Raman (using visible light) detection techniques, the device must be optically transparent. For infrared detection, the device must be transparent to infrared radiation wavelengths	For 1-dimensional concentration profiles, the measurement is representative of the concentration averaged through the depth of the channel or device. It is pertinent only if the flow structure is 2-dimensional and the concentrations are constant throughout the depth of the channel. Appropriate for single and two phase systems	Hessel et al. (2003), Masca et al. (2006), Salmon et al. (2005), Cristobal et al. (2006)

longer side-by-side but layered on top of one another, which presents a problem in determining the true point of complete mixing since the dye concentration is averaged through the depth of the microchannel. Another example of this is given by Lee et al. (2006), who present the mixing of a blue dye solution with water in a split-and-recombine mixer as shown in Fig. 1(d). As the blue stream is split and then superimposed the colour intensity oscillates but does not give any spatial information about the mixing quality throughout the depth of the micromixer.

2.1.1.2. Dilution of fluorescent species. When using fluorescent dyes, high energy light (e.g. laser) is required to induce fluorescence, which is monitored using fluorescence microscopy. Typical fluorescent dyes are fluorescein and rhodamine B. An advantage of this particular method is that it is possible to obtain spatial information on the dye concentration throughout the depth of the microchannel if a confocal scanning laser microscope (CSLM) is used. CSLM enables point measurement of the fluorescent dye across the microchannel cross section and allows 3-dimensional data to be retrieved, as will be shown in Fig. 2.

Fig. 2 shows some examples of visualising mixing in microchannels using fluorescent dyes. The examples cited in Figs. 2(a) (Johnson et al., 2002) and 2(b) (Knight et al., 1998) employ conventional fluorescence microscopy whereby the visualisation of the mixing process is conducted perpendicular to the flow in T- and hydrodynamic focusing micromixers. The resulting images provide information on the fluorophore concentration that is averaged over the depth of the microchannel. This may be a limitation in micromixers that create three-dimensional mixing patterns, resulting in some apparent 'smearing' of the marked species across the microchannel and consequently overly short mixing lengths. In mixers whereby a multi-layered mixing pattern is created, fluorescent imaging using confocal scanning microscopy may be preferred. This technique enables scanning pointwise measurements of the fluorescent dye throughout the depth of the micromixer and allows information on the scale of segregation to be retrieved. Figs. 2(c–e) show examples of fluorescent imaging using scanning confocal microscopy in hydrodynamic focusing (Knight et al., 1998), T-junction (Hoffmann et al., 2006) and chaotic (Stroock et al., 2002) micromixer geometries, respectively. The highly complex 3-dimensional mixing patterns created in the T-junction and chaotic micromixers (Figs. 2(d–e)) highlights the importance of resolving the tracer concentration fields throughout the depth of the microchannel, which allows the distribution of striation thicknesses and therefore the length scales of the system to be determined.

2.1.2. Reaction-based characterisation methods

Three types of reaction-based characterisation methods exist: acid-base reactions, reactions producing a coloured species and competing parallel reactions. These methods rely on contacting two reactant streams, which upon mixing and reaction produce a colour change, or a coloured or analytically detectable product. These methods characterise the intensity of segregation at the molecular scale, providing thus information on micro-mixing reactions inducing a change in colour.

The measurement principals and technical requirements of acid-base and coloured specie reactions are very similar to those of the dilution-base characterisation methods. A change in colour due to reaction is monitored using conventional imaging techniques, which means that there must be optical access to the flow. Mixing is typically judged complete in a qualitative manner when there is no further colour evolution across the mixer cross-section. Again, since these methods employ conventional microscopy, information on the spatial mixing quality in the mixer cross section is not accessible, and therefore may be less adapted to complex 3-dimensional mixing processes.

2.1.2.1. Acid-base or pH indicator reactions. The generation of colour change in acid-base reactions relies on the presence of a pH indicator in the basic or acidic solution. A number of different pH indicators have been used for characterising mixing in micromixers and the choice of indicator mainly relies on the contrast of the resulting colour change. Schwesinger et al. (1996) contacted aqueous solutions of chloric acid and pH indicator methyl orange in a split-and-recombine micromixer. In solutions with pH>4.4, methyl orange is yellow in colour and turns red in highly acidic solutions ($pH < 3.1$). A solution of pH indicator bromothymol blue, which is slightly yellow in acidic solution, and a transparent sodium hydroxide solution were used to examine mixing in zig-zag microchannels (Branebjerg et al., 1995). These solutions react instantaneously forming a rich blue colour, since bromothymol becomes blue in alkaline solutions. From these visualisation experiments, Branebjerg et al. (1995) estimated a mixing time by recording the time of colour change. Kockmann et al. (2006) have used the same pH indicator to evaluate the performance of various micromixer elements integrated onto a silicon chip. The mixing length was determined as the downstream length in the mixer where colour change was no longer visible. To estimate mixing time, the mixing length was divided by the average flow velocity. Another commonly used pH indicator in micromixer studies is the phenolphthalein indicator. The mixing performance in various designs of split-and-recombine and chaotic micromixers has been assessed by contacting water or ethanol solutions of phenolphthalein and sodium hydroxide (Liu et al., 2000; Kim et al., 2004; Cha et al., 2006; Lee et al., 2006). Phenolphthalein is colourless in acidic or near-neutral solutions ($pH < 8.2$) and turns pink in basic solutions. Examples of results using the phenolphthalein indicator are given in Fig. 3. Fig. 3(a) shows grey scale images taken from Liu et al. (2000) in a micromixer, which has viewing windows that are perpendicular to the flow direction. These images highlight the formation of the pink colour (shown as dark grey) at the interface of the two solutions and the complex structure of this interface throughout the depth of the channel. After two mixing elements of the chaotic micromixer, the colour is uniform and mixing is considered complete. Figs. 3(b–d), taken from Cha et al. (2006), Kim et al. (2004) and Lee et al. (2006) respectively, show colour images of the phenolphthalein indicator reaction in different split-and-recombine mixers. Layered fluid flow structures are evident in these and care must be taken in the analysis of data and the determination of the endpoint in mixing.

It should be pointed out that some care must be taken when comparing the performance of different devices or operating conditions since different results may be obtained if different acid/base concentration ratios are used. Furthermore, the quality and the resolution of the images are also important for the evaluation of mixing performance and determination of the endpoint, especially if a statistical analysis (e.g. calculation of the coefficient of variance) is done on the concentration field.

2.1.2.2. Reactions yielding coloured species. Ultimately, different reactions resulting in the formation of a coloured specie can be used for characterising mixing using this method; however, a practical requirement of the test reaction is the formation of a soluble coloured species. One test reaction reported in the literature to characterise a split-and-recombine micromixer is the reduction of potassium permanganate in alkaline ethanol (Mensinger et al., 1995). The initial reacting solution is purple and changes to green as manganate is formed, and then to a yellow-brown colour when the final compound manganese dioxide is

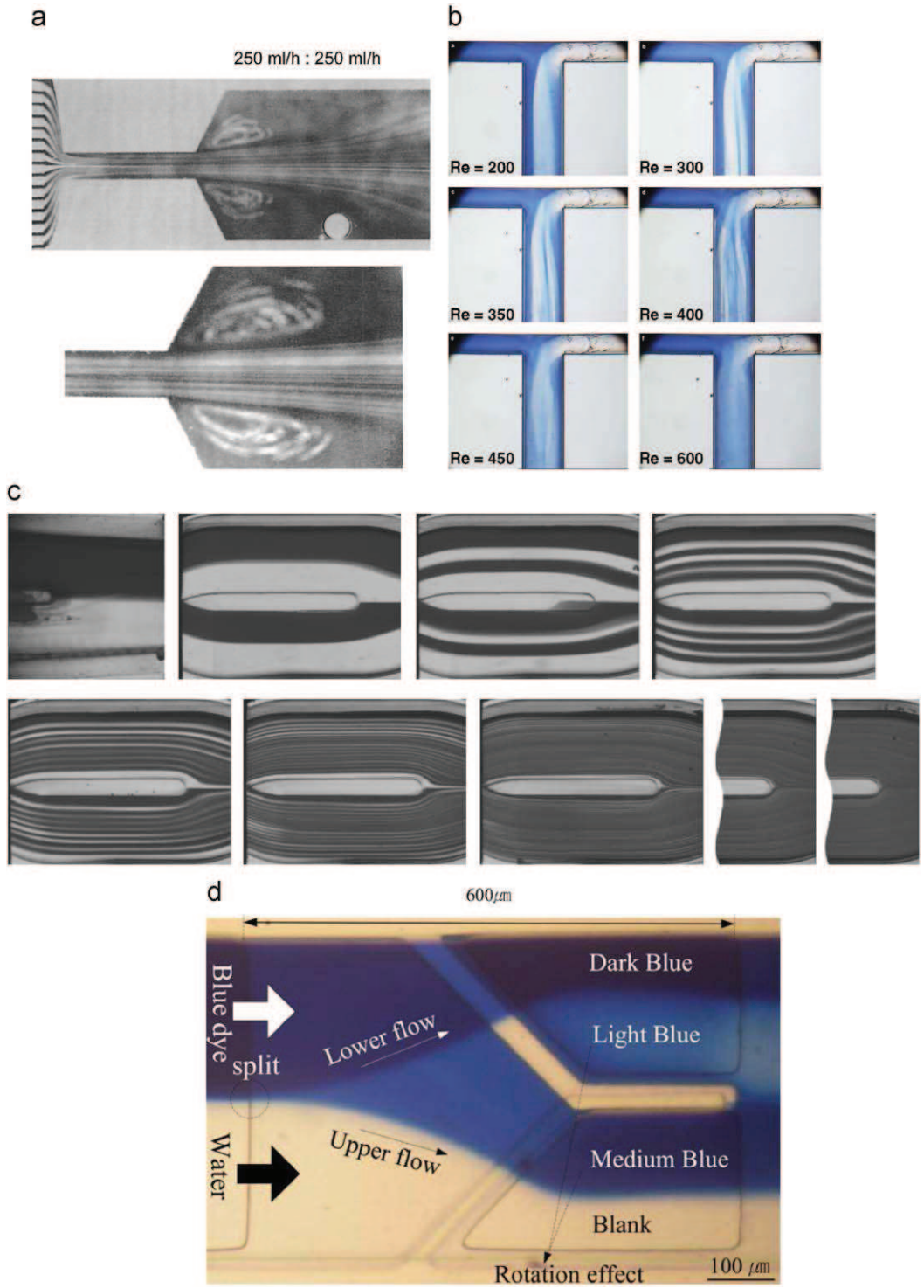

Fig. 1. Examples of diluting dyed fluid streams to characterise mixing quality: (a) Contacting of high concentrations of blue water and pure water in a multilamination hydrodynamic focusing micromixer followed by a sudden expansion (Hessel et al., 2003; reproduced with permission); (b) Mixing of a commercial blue coloured dye solution and deionized water in a T-mixer at different Reynolds numbers (Wong et al., 2004; reproduced with permission); (c) Contacting of a dyed solution (water-blue) (dark lamellae) and a transparent solution of 85% glycerol (light lamellae) in a split and recombine mixer (Schönfeld et al., 2004; reproduced with permission); (d) Mixing of a blue dye solution and water in a split-and-recombine micromixer. It can be see that when the blue streams are superimposed, the colour intensity changes and thus illustrating the difficulty in differentiating layered flow and well-mixed states with this simple dilution method (Lee et al., 2006; reproduced with permission). (For ı, the reader is referred to the web version of this article.)

formed. A disadvantage of this reaction is the formation of a solid product, which necessitates the cleaning of the micromixer with sulphuric acid. Another test reaction is the iron rhodanide reaction, which has been used to characterise mixing in interdigital (Hessel et al., 2003) and split-and-recombine (Hardt et al., 2006) micromixers. An example of the visual results obtained is given in Fig. 4. In this reaction, a transparent colourless solution containing SCN^- (thiocyanate) ions is reacted with a transparent but slightly yellow solution containing Fe^{3+} ions to form a dark reddish brown compound. In Fig. 4, the product ferric

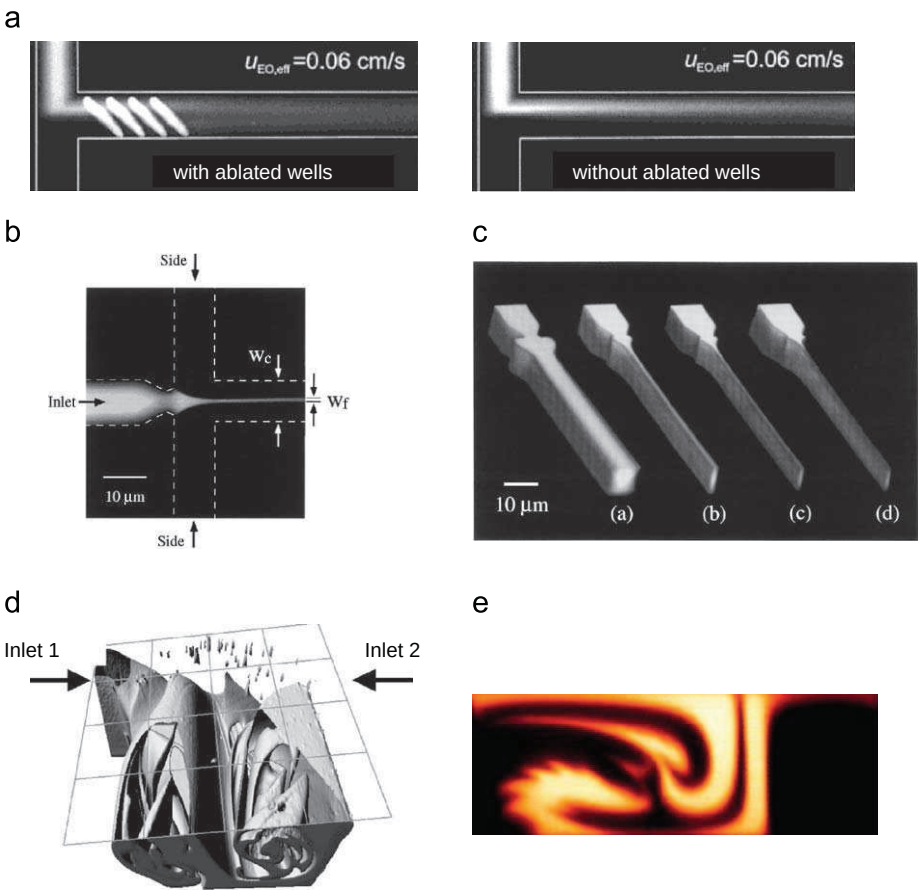

Fig. 2. Examples of visualising the dilution of fluorescent dyes to characterise mixing: (a) Fluorescence microscopy using rhodamine B in a T-mixer with (left) and without (right) ablated wells (Johnson et al., 2002; reproduced with permission); (b) Dilution of a fluorescein solution in a hydrodynamic focusing geometry visualised by fluorescence microscopy (Knight et al., 1998; reproduced with permission); (c) Three dimensional images of fluorescein in a hydrodynamic focusing geometry visualised by confocal scanning microscopy (Knight et al., 1998; reproduced with permission); (d) Three dimensional concentration maps of rhodamine B entering via inlet 1 in a T-mixer, visualised by confocal scanning microscopy (Hoffmann et al., 2006; reproduced with permission); (e) Mixing patterns in the cross section of a chaotic micromixer visualised using fluorescein and confocal scanning microscopy (Stroock et al., 2002; reproduced with permission).

thiocyanate is clearly visible as dark lines at the interface of the reactants. The advantage of this reaction over the dilution-based methods is that the coloured product only appears once the reactants are completely mixed at the molecular scale. The drawback, which is inherent to the conventional imaging and microscopic techniques employed for visualisation, is that no information on the spatial mixing quality throughout the depth of the micromixer can be obtained, which can lead the under- or over-estimation of mixing times/lengths.

2.1.2.3. Competing parallel reactions. The principle of this method is to carry out two reactions in parallel that both use a common reactant, which they compete for. One of the reactions should be very fast, and therefore proceeds only if mixing is ideal (i.e. extremely rapid). The other reaction should be fast (but slower than the first reaction) and it takes place when there is an excess of the common reactant, i.e. when mixing is slow and non-ideal. Quantitative information can be obtained on the yield of the secondary (slower) reaction. Consequently, mixing performance is characterised by the amount of secondary product formed: the greater the yield of the secondary reaction, the poorer the micromixing quality.

Two types of competing parallel reaction systems have been reported for characterising mixing in micromixers. The first reactive system is known as the Villermaux/Dushman or the iodide-iodate method. This method is based on a technique originally developed for the characterisation of micromixing in stirred tanks (Fournier et al., 1996; Guichardon and Falk, 2000) and has been the most commonly used method for evaluating micromixer performance (Ehrfeld et al., 1999; Keoschkerjan et al., 2004; Panic et al., 2004; Nagasawa et al., 2005; Aoki and Mae, 2006; Kockmann et al., 2006). The first reaction (1) is the neutralisation of an acid, which is an almost instantaneous process. The second slower process is the reaction (2) of potassium iodide with potassium iodate, which is catalysed by an acid to form iodine.

$$H_2BO_3^- + H^+ \Leftrightarrow H_3BO_3 \quad (1)$$

$$5I^- + IO_3^- + 6H^+ \Leftrightarrow 3I_2 + 3H_2O \quad (2)$$

In the case where mixing is slow, the first reaction is not complete and there is an excess of acid (H^+). This acid catalyses the second reaction and thus promotes the formation of detectable iodine. The amount of iodine formed is detected as a tri-iodide complex using an ultraviolet–visible (UV–Vis) spectrometer; the tri-iodide complex has its characteristic absorption bands centred at 286 and 353 nm, which are in the upper UV spectrum. For on-line UV–Vis spectroscopic measurements, a transparent micromixer or measurement cell is required. Off-line measurements are also possible; however care must be taken as long time delays between sampling and analysis may promote the secondary reaction if mixing is not complete in the micromixer. From the

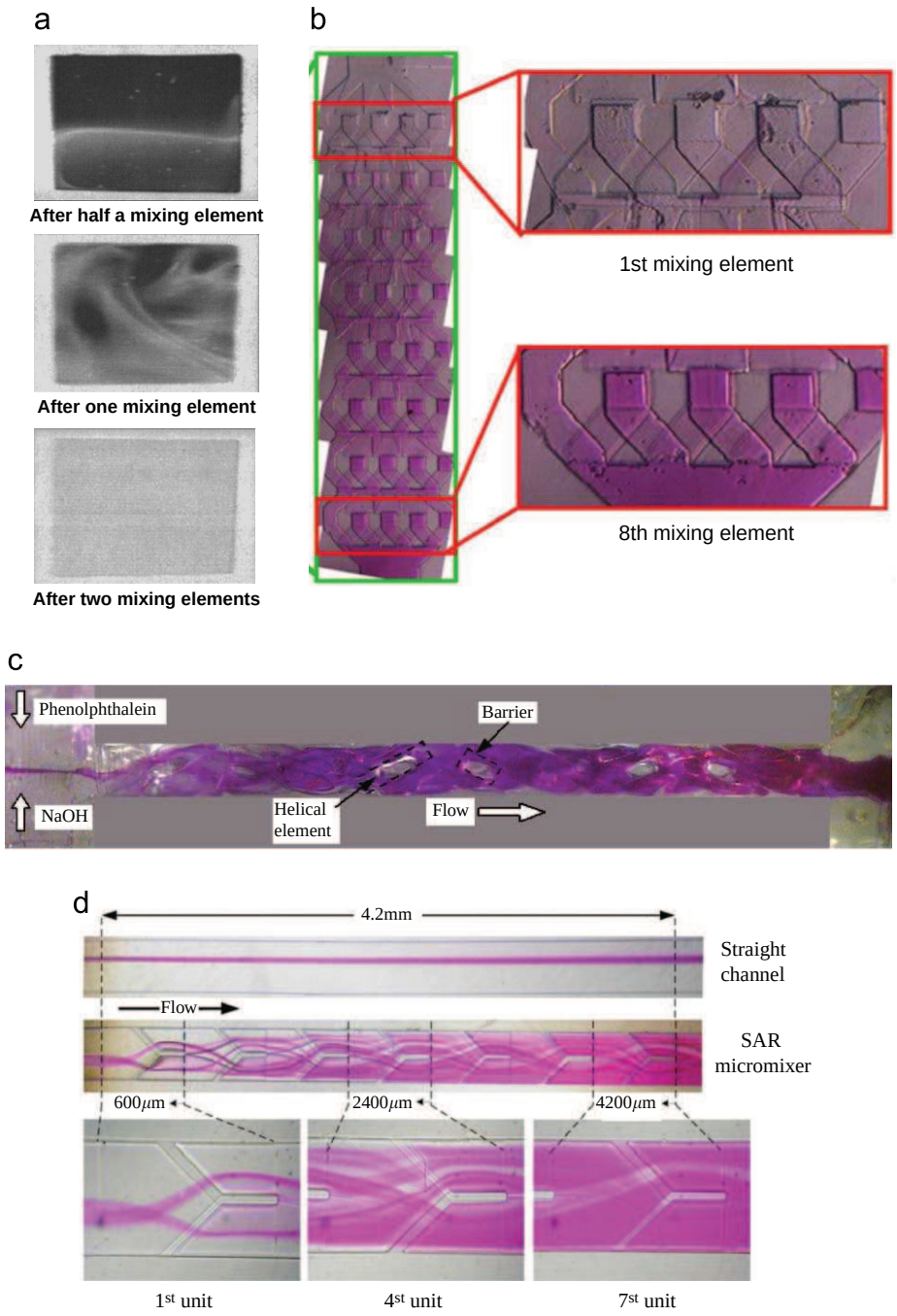

Fig. 3. Examples of characterising mixing quality using the phenolphthalein pH indicator reaction: (a) Cross sectional slices showing the mixing of phenolphthalein and sodium hydroxide in ethanol solutions in a passive serpentine micromixer—the formation of the pink indicator is represented by the dark grey scale (Liu et al., 2000; reproduced with permission); (b) Mixing is shown to be complete when the pink colour remains constant, this is after the 7th mixing element in this split-and-recombine micromixer (Cha et al., 2006; reproduced with permission); (c) Mixing and the acid-base reaction in a barrier embedded Kenics micromixer (Kim et al., 2004; reproduced with permission); (d) Mixing performance in a straight microchannel and a split-and-recombine micromixer. The latter illustrates the effectiveness of these 3-dimensional geometries, which promote convection and mixing by stretching and folding the miscible fluid interface (Lee et al., 2006; reproduced with permission). (For interpretation of the references to color in this figure legend, the reader is referred to the web version of this article.)

measurement of iodine concentration, the performance of micromixers has most often been compared on the basis of the segregation index, as defined in the original experimental protocol (Guichardon and Falk, 2000). This index returns a value between 0 for perfectly mixed systems and 1 for totally segregated systems. The mixing time in a particular device can further be determined with knowledge of the segregation index and the use of an additional mixing model (Falk and Commenge, 2010). It is important to point out that the segregation index is a function of the experimental protocol since the amount of iodine formed depends strongly on the concentration of the acid reactant and therefore the pH of the reacting solution. Therefore, in order to obtain iodine measurements that are sensitive enough to distinguish different mixing performances, the acid concentrations in the experimental protocol must be adapted to the flow rates employed in the micromixer (Panic et al., 2004). As a result, it is recommended that the same reaction conditions are used when relatively comparing micromixer devices.

The second competing parallel reaction system that has been used for characterising the mixing performance of different

Fig. 4. Characterising mixing in a split-and-recombine micromixer with a reaction generating a coloured compound (Hardt et al., 2006; reproduced with permission). The reaction used here is between a transparent colourless solution containing SCN^- (thiocyanate) ions and a transparent but slightly yellow solution containing Fe^{3+} ions to form a dark reddish brown compound at the interface of the reactant solutions. (For interpretation of the references to color in this figure legend, the reader is referred to the web version of this article.)

microreactors is the simultaneous diazo coupling of 1- and 2-napthol with diazotized sulfanilic acid. This is known as the second Bourne reaction scheme and was also originally developed for studying micromixing in stirred tanks (Bourne et al., 1992). The primary reaction (3) of 1-naphthol and diazotized sulfanilic acid is very fast and produces two isomers. The secondary reaction (4) involving 2-naphthol is about 100 times slower than reaction (3) and produces a third isomer.

$$\text{1-Naphthol} + \text{diazotized sulfanilic acid} \rightarrow \text{isomer o-R} + \text{isomer p-R} \quad (3)$$

$$\text{2-Naphthol} + \text{diazotized sulfanilic acid} \rightarrow \text{isomer Q} \quad (4)$$

In the case of slow mixing, the primary reaction is not complete and the diazotized sulfanilic acid continues to react with the 2-naphthol. The ratio of isomer Q to isomers R increases with decreasing mixing efficiency. The amounts of R and Q isomers produced are measured by UV-spectrophotometry, which as mentioned above requires a transparent micromixer for on-line measurements or a transparent measuring cell for off-line acquisition. Although this reaction system has been successfully applied to characterize the performance of a micro-jetmixer (Ehlers et al., 2000) it is relatively difficult to use, which explains the preference for the Villermaux/Dushmann method using the protocol given by Panic et al. (2004).

2.1.3. Monitoring of species concentration

The spatial or temporal *in-situ* monitoring of species concentration is a quantitative method for measuring mixing and is one largely used when evaluating the performance of stirred tanks and macro-scale static mixers via the coefficient of variance (Paul et al., 2004). Sampling may be carried out on a line transect in order to obtain a 1-dimensional concentration profile, over a plane in the flow to obtain 2-dimensional concentration fields, or at a point. For all three sampling strategies, the temporal or spatial mean and variance can be calculated to give a measure of the intensity of segregation and therefore the 'evenness' of concentration. However, the purpose of a transect is most often to profile concentration and to determine a striation thickness distribution, thus giving information about the scales of segregation. In micromixing devices, the detection of the species concentration is typically carried out using photometric and fluorescence methods, as well as Raman (Vis, UV, IR) techniques. These measurement techniques require an optically transparent micro device or one that is transparent to IR radiation in the case of IR Raman.

Fig. 5 shows examples of concentration measurements in micromixers using various detection methods. Hessel et al. (2003) quantified mixing (dilution of blue dye) in an interdigital micromixer by plotting 1-dimensional concentration profiles taken along a transect that is projected over the cross-section of the micromixer, as shown in Fig. 5(a). This measurement is representative of the concentration averaged over the depth of the channel or device. In the case of the interdigital micromixer presented in the study, this type of concentration measurement is pertinent since the flow structure is primarily 2-dimensional and the blue dye concentrations are constant throughout the depth of the channel. As a result, the concentration profiles give direct information on the thickness of the fluid lamellae. In the case of more complex layered 3-dimensional flows, the same profiles would be less meaningful since the real concentration gradients throughout the depth of the device would be smeared in the 1-dimensional profile. For such flows, it would be more appropriate to extract a plane of concentration data, such as that shown in Fig. 2(d, e), and then conduct analysis on the whole volume or plane of data, or along selected line transects. In addition to confocal fluorescence microscopy used to obtain the concentration fields shown in Fig. 2(d, e), Raman spectroscopy is another technique that enables the measurement of local concentrations of chemical species. Masca et al. (2006) demonstrate the use of ultraviolet resonance Raman spectroscopy to follow mixing via the evolution of species concentration at different points in a T-micromixer. Fig. 5(b) shows concentration profiles measured using scanning confocal Raman microspectroscopy in a simple Y-micromixer (Salmon et al., 2005). In these experiments, the height of the sampling volume was much greater than the depth of the microchannel. As a result the Raman spectra are averaged over the channel depth. The concentration profiles are however pertinent since in this case a large aspect ratio channel (channel width $\gg$ channel depth) was used and the flow is essentially 2-dimensional.

2.2. Hydrodynamics

The mixing performance in all types of reactors and mixers is highly dependent on the flow occurring within the device. In order to better understand the mixing phenomena, the hydrodynamics in the device must be known. To characterise local hydrodynamics in micro devices, a number of methods can be used; most of these have been adapted from conventional macro scale techniques.

2.2.1. Micro particle image velocimetry (μ-PIV)

Micro particle image velocimetry (μ-PIV) has been developed specifically for the determination of instantaneous fluid velocity fields within microchannels (Santiago et al., 1998; Meinhart et al., 1999). It is a non-intrusive optical technique that enables local analysis of the flow at a high spatial resolution (down to $\sim$1 μm). The principals of μ-PIV are based on those of conventional PIV: micro-sized seeding particles are introduced into the flow and illuminated by laser light; two successive images (separated by a very short time interval) of the particles are then taken; these two particle images are correlated in order to determine the distance travelled by the particles during the time interval and subsequently, the instantaneous velocity field in the flow. However, in contrast to conventional PIV, the entire volume of the

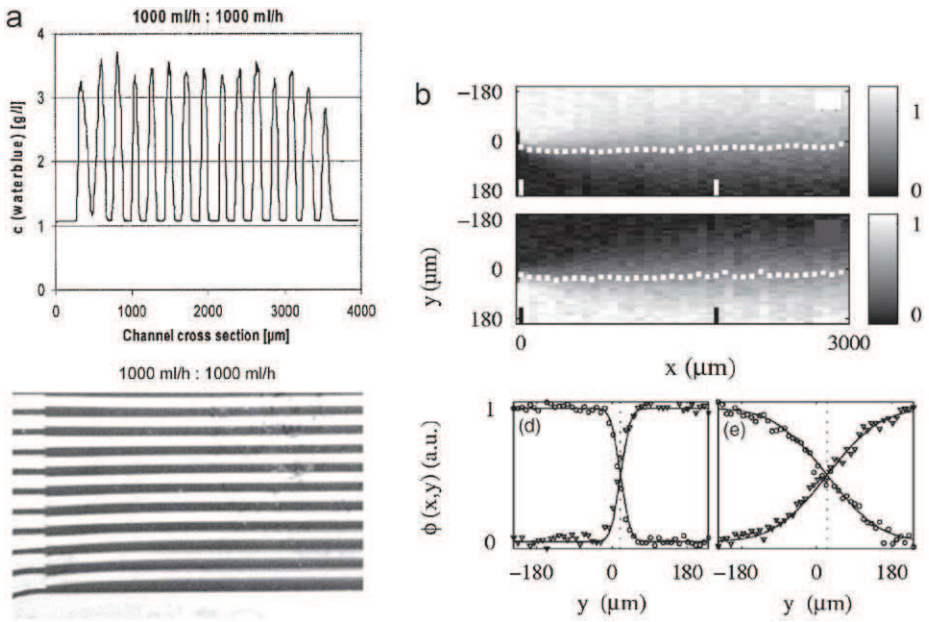

Fig. 5. Examples of monitoring the concentration of chemical species in microdevices: (a) Concentration profiles on a transect across an interdigital micromixer (right) taken from dilution-based visualisation experiments (left) (Hessel et al., 2003; reproduced with permission). Since the flow in this type of micromixer is essentially 2-dimensional, the concentration profile provides information on the thickness of the fluid lamellae. (b) Two dimensional Raman images of chloroform (top) and methylene chloride (middle) taken along the length of a Y-micromixer (Salmon et al., 2005; reproduced with permission). The corresponding concentration profiles (bottom) of the chloroform (○) and methylene chloride (▼) taken at $x \approx 45$ and $x \approx 1800\,\mu m$ are representative of the species concentration averaged through the depth of the microchannel.

microchannel flow is illuminated in μ-PIV and a microscope is used to focus on a near 2-dimensional measuring plane, whereby the velocity field is determined. Typically, two in-plane velocity components are measured.

As for other optical measurement methods described in this article, μ-PIV requires that the microdevice is transparent or is at least equipped with a transparent viewing window in the region of interest. Furthermore, when applying μ-PIV to characterise a flow, there are a number of additional technical aspects to consider. Firstly, the μ-PIV technique relies on images of tracer particles that seed the flow. Due to the small dimensions of microchannel devices, an appropriate seeding particle size must be chosen such that it is small enough to avoid channel clogging but large enough to emit light with sufficient intensity. Secondly, the resolution of the measurements, the field of view, as well as the working distance (distance between the measurement plane and the objective) are determined primarily by the magnification and the numerical aperture of the microscope objective. Generally, as the magnification (M) and the numerical aperture (NA) of the objective increase, the depth of correlation (thickness of the measurement plane), the working distance and the measurement field size decrease. For example, with a $10\times/0.3$ (M/NA) objective, the depth of correlation is $\sim 27\,\mu m$, the working distance is approximately 6 mm and the field of view $\sim 1\,mm^2$. On the other hand, with a $40\times/0.6$ objective the spatial depth-wise resolution is approximately $6\,\mu m$, however the working distance and the field of view are reduced to $< 3\,mm$ and $200\times 200\,\mu m^2$, respectively. With higher magnification, there is a gain in the spatial resolution of the measurement; however the measurement plane in the micro device must be very close to the microscope objective, which is often technically difficult due to obstructions by the inlet and outlet tubing and the thickness of the transparent reactor wall. Measurements taken with objectives of lower magnification are technically easier to set-up as the working distance is larger. However, in such cases, the depth of correlation is often the similar, to or larger, than the depth of the microchannel and therefore the measured velocity field represents an average of the flow field throughout the depth of the microchannel.

There are now a large number of literature examples that employ μ-PIV for characterising hydrodynamics in micro channel devices. Fig. 6 presents a selection of these studies that particularly concern micromixers. Fig. 6(a) shows the velocity profiles of water and diluted glycerol contacted in a hydrodynamic focusing micromixer whereby two outer sheath streams of one fluid focus on a central sample stream (Wu and Nguyen, 2005). In these experiments, a $4\times$ objective was used to measure the velocity fields in a wide shallow microchannel ($900\,\mu m \times 50\,\mu m$). Consequently, the depth of measurement is relatively large and the velocity fields represent an average throughout the channel depth. By seeding both the viscous glycerol stream and the water stream, the measurements enable a quantitative assessment of the flow patterns when equal stream flow rates are used. Hoffmann et al. (2006) have employed μ-PIV to investigate the effects of high laminar flow Reynolds numbers on the flow in T-micromixers (Fig. 6(b)). They used a $20\times/0.4$ objective which gives approximately a $13\,\mu m$ measurement depth to determine flow fields in 100 and $200\,\mu m$ deep channels. This small measurement depth thus allows several planes of measurement throughout the channel depth. Fig. 6(b) compares the velocity profile at the centre plane for a Reynolds number of 120 (left), where the velocity profile is parabolic, with that of a Reynolds number of 186 (right) where the velocity profile in no longer parabolic due to the transition to engulfment flow. Fig. 6(c) presents an instantaneous 2-dimensional velocity field in a micromixing device based on the time dependent pulsing of flow via secondary channels (Bottausci et al., 2007). The μ-PIV measurements capture the formation of two recirculation vortices due to the pulse flow from the side channels, which enable the high-speed mixing of two fluid streams.

It is also worthwhile pointing out some of the developments being made in μ-PIV that deal with the limitations and associated

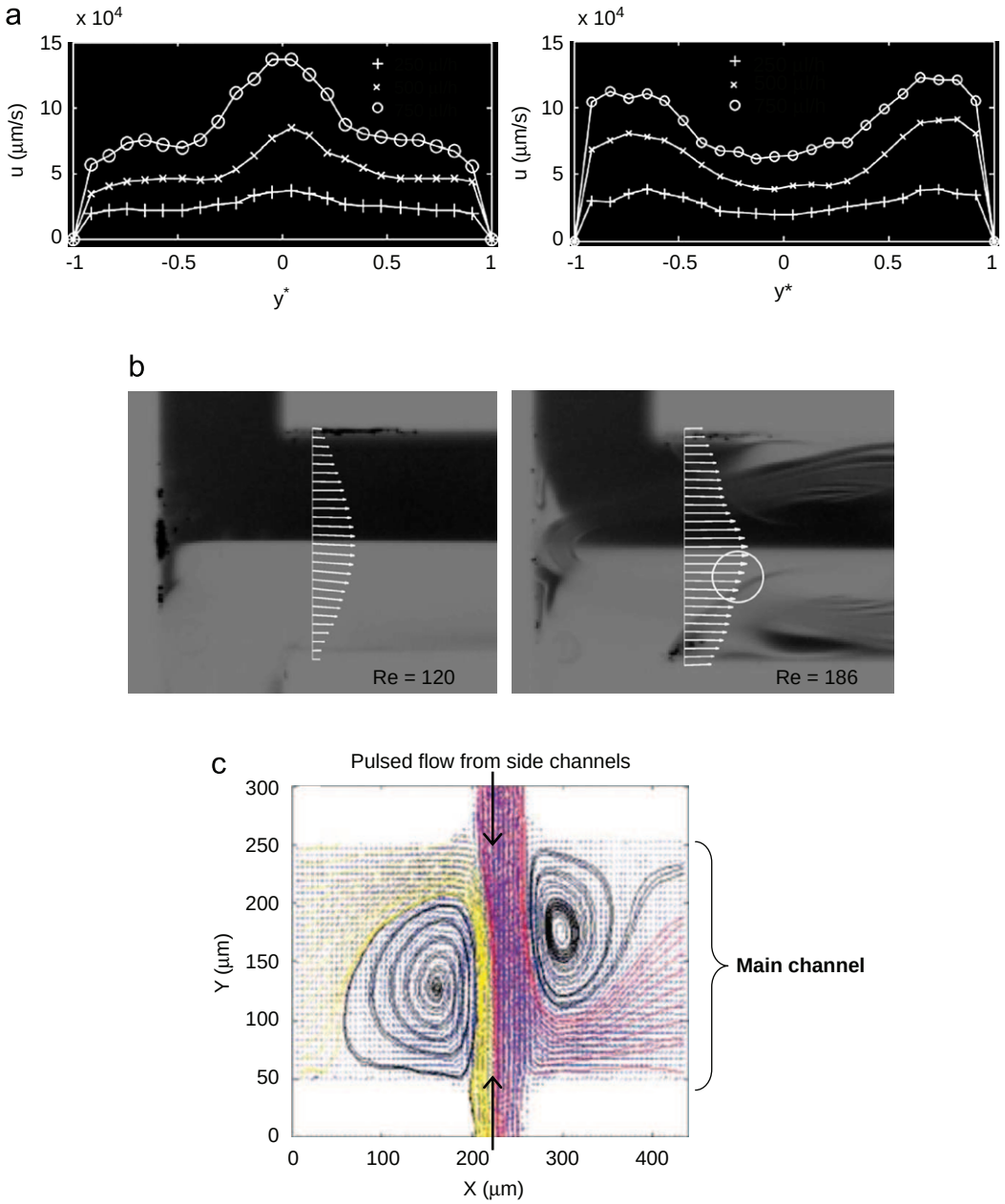

Fig. 6. Examples of 2-dimensional velocity measurements by μ-PIV. (a) Velocity profiles of water and diluted glycerol contacted in a hydrodynamic focusing micromixer at different flow rates (Wu and Nguyen, 2005; reproduced with permission). The inlet flow rates of all streams are equal and the viscosity of the glycerol solution is 1.8 times that of water. Left: the central flow is water and is focused by two outer sheath flows of glycerol solution. Right: the central flow is diluted glycerol, which is focused by two outer sheath flows of water. (b)Velocity profiles at the centre plane of a T-micromixer (Hoffmann et al., 2006; reproduced with permission). At Re=120 (left), the velocity profile is parabolic. When the flow rate increases and the transition to engulfment flow is reached (Re>160), the velocity profile changes and mixing is enhanced. (c) Flow patterns in a pulsed injection micromixer (Bottausci et al., 2007; reproduced with permission). The creation of time dependent vortices in the main channel by the pulsed flow coming from the side channels provides a means for high-speed mixing.

difficulties of the technique. As mentioned above, μ-PIV requires optical access to the microchannel flow. To overcome this limitation when using non-optically transparent silicon-based microdevices, Liu et al. (2005) have developed infrared μ-PIV for the measurement of flow fields. Silicon is relatively transparent in the near-infrared waveband, which means that measurements can be made through the silicon using an infrared illumination source without the need for optical windows. μ-PIV measurements provide instantaneous planar velocity fields that generally comprise two in-plane velocity components. However, in many of the efficient micromixer geometries available on the market or presented in the literature, the flows created are 3-dimensional. As a result, a complete characterisation of the flow is not possible experimentally. The development of stereoscopic μ-PIV, which employs two cameras positioned at an angle to one another and a stereomicroscope, enables the simultaneous measurement of all three velocity components on the measurement plane. Lindken et al. (2006) developed a stereoscopic μ-PIV system and performed measurements in a T-shaped micromixer providing a full 3-dimensional scan of the velocity field, as shown in Fig. 7(a). With the stereoscopic equipment used, nine velocity planes were measured throughout the channel height of 200 μm. Bown et al. (2006) have carried out stereoscopic μ-PIV experiments to determine the 3-dimensional velocity field of

flow over a micro-step in a microchannel. Three component velocity fields are determined on 23 equally spaced planes through the 466 μm deep channel, just downstream of the step (Fig. 7(b)). In most of the flow field, the measurements agree with a CFD solution of the flow within the experimental uncertainties. However, the authors do point out that the accuracy of the out-of-plane velocity measurement is restricted by the misalignment of the two focal planes in the stereomicroscope.

2.2.2. Micro particle tracking velocimetry (μ-PTV)

In μ-PTV the velocity field in a plane is determined by tracking individual particles from image to image, instead of cross-correlating the displacement of a group of particles in a selected interrogation area as done in PIV. This results in a two-component velocity field with an enhanced spatial resolution compared with that obtained using μ-PIV, since in principle a velocity vector is obtained for each particle tracked. In order to correctly identify each particle from image to image, typically a low seeding density is required. However, the use of 'super resolution' algorithms that employ PIV cross-correlation in a first step to guide PTV particle matching in a second step enables a higher density seeding to be used, and results in a higher resolution of the velocity fields. An example of this is given by Devasenathipathy et al. (2003). They have used μ-PTV with a super resolution algorithm to determine two-component planar velocity fields in a micro cross-channel system. Fig. 8 shows the superior spatial resolution of the flow that is obtained by tracking individual particles with μ-PTV (right) compared with μ-PIV (left). In addition to the improvements made in the resolution of μ-PTV measurements, developments have also been made to simultaneously map 3-dimensional velocity fields. Stereoscopic μ-PTV uses two cameras to track the 3-dimensional coordinates of individual particles and determine the 3-component flow field. In a channel with a micro-step, Bown et al. (2006) have shown that the scatter in velocities of individual particle tracks can be reduced by the 3-dimensional averaging of velocities over small control volumes. Since the size and position of the control volumes can be set by the user and the particles belong to a particular control volume based on their 3-dimensional position, the out-of-plane resolution of the measurement is no longer dependent on the microscope objective used. Park and Kihm (2006) developed an alternate three-dimensional μ-PTV technique that uses a single camera with deconvolution microscopy. This method tracks the out-of-plane location of the seeding particles by correlating the diffraction ring pattern size of the particles with the defocus distance from the focal plane. Using a $40\times/0.75$ objective, the authors demonstrated highly resolved ($5.16\,\mu m \times 5.16\,\mu m \times 5.16\,\mu m$) measurements of the three velocity components in a $100\,\mu m \times 100\,\mu m$ section microchannel.

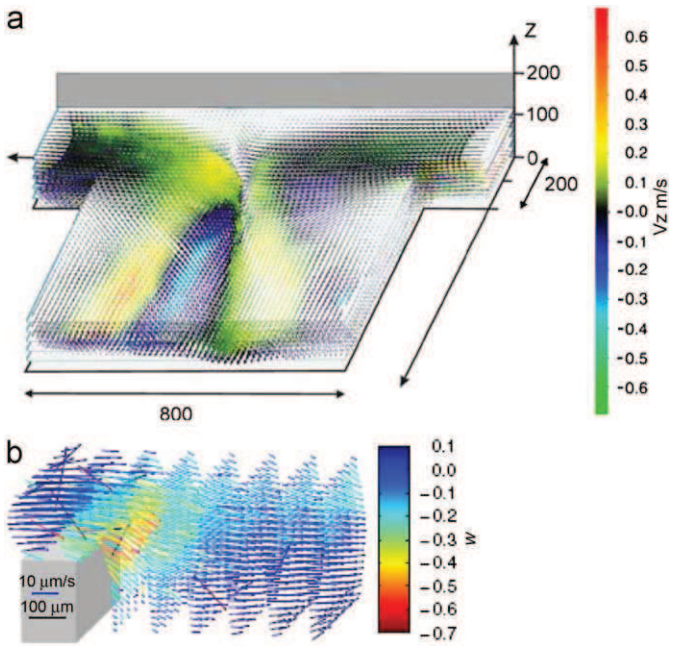

Fig. 7. Examples of stereoscopic μ-PIV measurements to obtain three-component velocity fields. (a) Three-dimensional scan of stereo-PIV measurements in the mixing zone of a T-mixer at Re=120 (Lindken et al., 2006; reproduced with permission). The vectors are coloured by the out-of-plane component. The velocity fields in the lower half of the micromixer are shown only. (b) Three-component vector map of the flow field across the micro-step at a resolution of $45 \times 45 \times 109$ μm (Bown et al., 2006; reproduced with permission). The vectors are coloured by their out-of-plane velocities. (For interpretation of the color bar legends in the figures, the reader is referred to the web version of this article.)

2.2.3. Molecular tagging velocimetry (MTV)

MTV relies on the use of special molecules that become tracers when exited by photons of an appropriated wavelength. A pulsed laser is used to excite and "tag" the molecules in particular regions of the flow. The displacement of these tagged fluid regions is then followed over time with sequential camera images. An algorithm, similar to that used in PIV, is employed to determine the velocities of the fluid regions by the spatial correlation of two successive images. For application in micro devices, laser light patterns the fluid by a mask that defines a line of tagged fluid or a grid of tagged fluid regions (Fig. 9(a)). When a line of fluid is tagged, only velocities normal to the line can be measured. However, tagging a grid of fluid regions enables a two-component 2-dimensional velocity field to be determined. Experimental constraints require that the device is optically transparent and that volume illumination of the flow has to be used, like that applied in PIV. Consequently, the tagged fluid regions are in fact small volumes of fluid and the resulting velocity field is averaged throughout the depth of the device, which limits the resolution of the measurement. Nevertheless, the advantage of MTV over the PIV and PTV techniques is that it does not require seeding particles and can offer significant gains when the presence of seeding particles can be detrimental to the operation of a device or the flow process. There are several examples of MTV along a single line in microchannel flows (see for example Maynes and Webb, 2002; Mosier et al., 2002); however the application of 2-dimensional MTV is more recent. Roetmann et al. (2008) have demonstrated the use of 2-dimensional MTV to measure the velocity fields within the mixing chamber ($5\,mm \times 5\,mm \times 200\,\mu m$) of a microfluidic device. Fig. 9(b) shows the time averaged velocity field of stationary flow in the mixing chamber obtained using 10 instantaneous velocity fields. In principle, an instantaneous vector field only contains vectors at pixels that belong to tagged regions of the flow, like those shown in Fig. 9(a). However, since the tagged regions move with time, the entire flow field becomes visible as the time averaging routine proceeds. These authors have also addressed the problem of spatial resolution throughout the depth of the microchannel with this type of measurement and the resulting effects on the quantitative evaluation of the flow field. This has led to the modification of the MTV algorithms for the determination of velocity values. The measured velocities are corrected such that they correspond to the velocities of a pure 2-dimensional velocity profile positioned in the middle of the channel. A quantitative comparison of the MTV measurements obtained with the modified algorithm with μ-PIV measurements performed in the same microchannel shows good agreement.

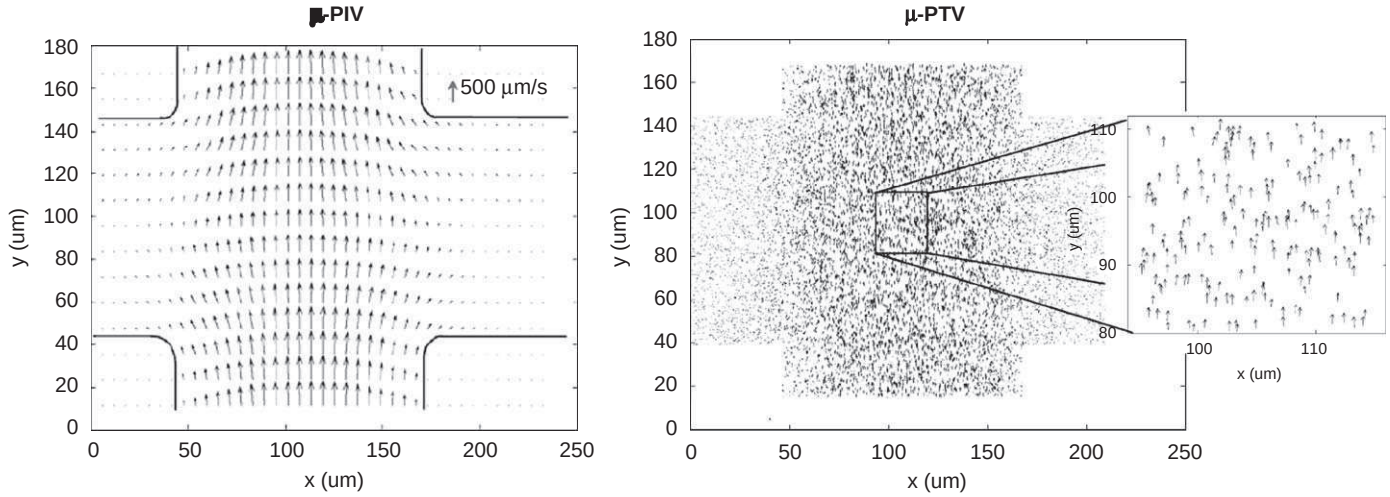

Fig. 8. A comparison of the spatial resolution of two-component velocity measurements using μ-PIV (left) and μ-PTV (right) (Devasenathipathy et al., 2003; reproduced with permission). Both velocity fields have been determined from the same particle images. The individual tracking of particles using super resolution algorithms for μ-PTV provide enhanced spatial resolution with over ten times more velocity vectors per unit area than μ-PIV measurements.

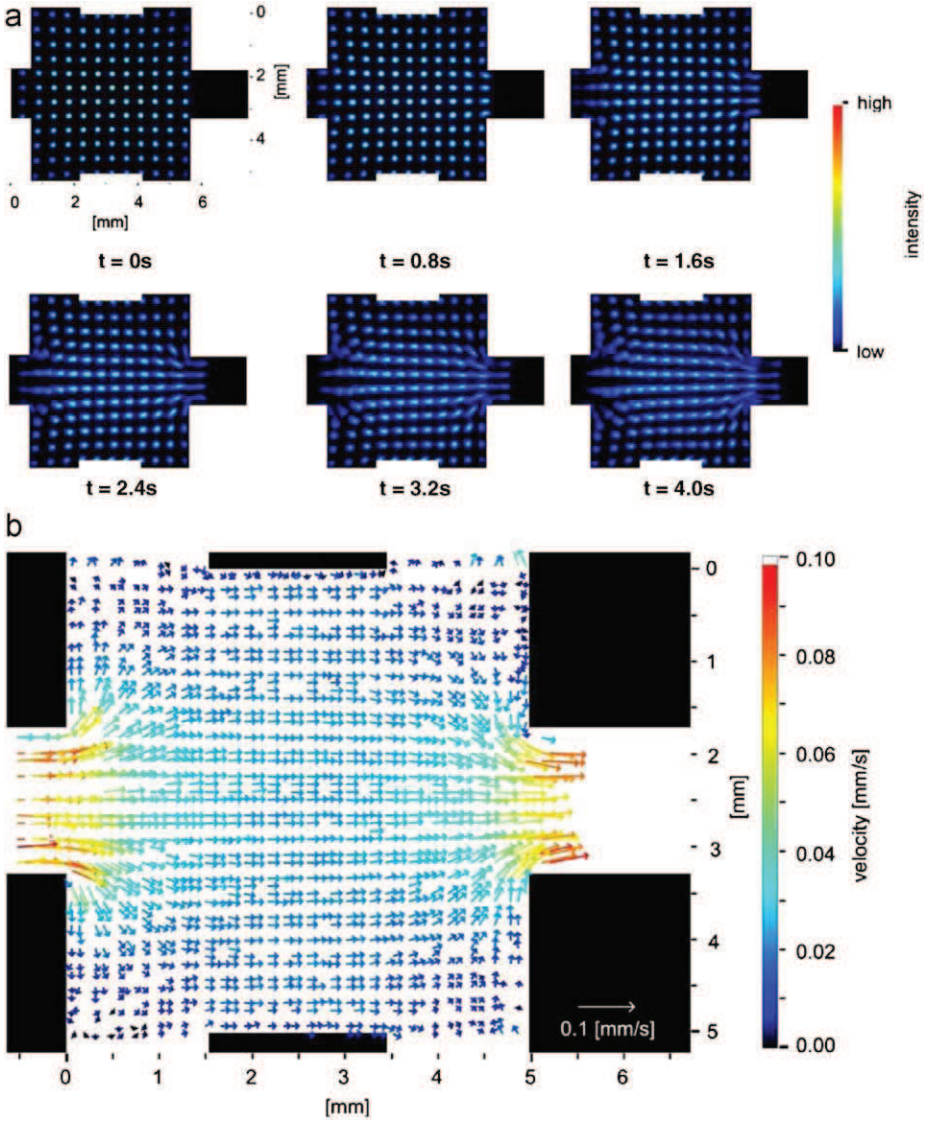

Fig. 9. Measurement of velocity fields in a micromixer using 2-dimensional MTV (Roetmann et al., 2008; reproduced with permission). (a) A series of images showing the temporal evolution of the displacement of tagged fluid regions in the micromixer. (b) The temporally averaged velocity vector field calculated from a series of 10 images, including those shown in (a). (For interpretation of the color bar legends in the figures, the reader is referred to the web version of this article.)

2.2.4. Electrodiffusion diagnostics

The electrodiffusion technique is one of only a few methods suitable for measuring the liquid velocity in close proximity of a wall. The principle is based on the measurement of the limiting electric current passing through a small electrode mounted flush with the wall of the experimental channel. A voltage applied to the electrochemical cell, represented by the working electrode and a larger counter electrode, drives a redox reaction at the electrode surfaces. Under the conditions for which the rate of the electrochemical reaction is fast enough to justify the assumption that the concentration of the reacting ions is zero at the working electrode, the measured current is fully controlled by the convective diffusion only. If the length of the electrode in the flow direction is sufficiently small, the concentration boundary layer on the working electrode is thin. The flow velocity varies linearly throughout the thickness of this boundary layer, whilst the measured current is proportional to the shear rate at the wall. The advantages of this non-invasive technique are that it can provide information on the shear stress distribution and the direction of the liquid flow very close to the channel wall, as well as mass transfer coefficients. This type of near-wall information is typically difficult to obtain with other measurement techniques like μ-PIV, μ-PTV and MTV. In addition, it does not require transparent fluids or devices since it relies on small probes built into the device. Although this technique is well established for the study of single phase flow in macro-scale applications (e.g. Mizushina, 1971; Hanratty and Campbell, 1983; Sobolík et al., 1998; Tihon et al., 2001, 2003, 2006), it has only recently been applied to the measurement of flows in miniaturised devices (Huchet et al., 2007). Huchet et al. (2007) have used the electrodiffusion method to characterize the local flow structure and the global wall mass transfer (liquid–solid) within a network of crossing minichannels. Fig. 10 shows the fluctuations of the near-wall shear rate, *FR*, measured by the electrodiffusion method as a function of the Reynolds number, which are used to identify the transitional zone between the laminar and turbulent flow regimes at different axial positions *x/H* in the minichannel network.

2.2.5. Nuclear magnetic resonance (NMR) velocity imaging

NMR imaging techniques are based on the interaction of the nuclear magnetic properties of atom nuclei with magnetic fields that leads to resonance phenomena to obtain an image. NMR imaging also allows the detection and quantification of motion which, in a simplified manner, can be determined by measuring the displacement of nuclear spins over a certain time. As a result, NMR imaging can provide an estimate of velocity fields. The details of NMR velocity imaging will not be given here, however, the readers are referred to Stapf and Han (2005) and Gladden et al. (2005) for introductory material on the technique and its application to chemical engineering problems.

NMR velocimetry is an established technique for characterising flow in large scale devices (see for example Stapf and Han, 2005), since it is an interesting alternative to other measurement methods. In addition to its non-intrusive nature, it allows local velocity measurements through both opaque and transparent media; in particular, it is advantageous for measurements in non-transparent fluids. Although measurements may be taken through opaque devices, NMR imaging is not compatible with magnetic or metallic materials. It is only recently that NMR velocity imaging has been applied to the flow in micro devices (Ahola et al., 2006; Raguin and Ciobanu, 2007). Ahola et al. (2006) have used NMR velocity imaging to measure velocity fields within a commercial interdigital micromixer made of glass. As shown in Fig. 11, the spatial resolution of the measurement (set by the size of the detector coil) was chosen such that the flow in the entire micromixer was imaged. Since in NMR velocity imaging the measured flow properties are pixel-averaged, the resolution used by Ahola et al. (2006) enabled the average velocity in each channel to be determined. However, since all microchannels were imaged simultaneously, heterogeneities in the flow distribution and local clogging in the mixer were clearly identified. The authors point out that by using a smaller detector coil, a higher resolution measurement can be obtained in the region of interest. Raguin and Ciobanu (2007) have also employed NMR velocity imaging to monitor average velocities in six parallel microchannels. In particular, they use a NMR technique that has

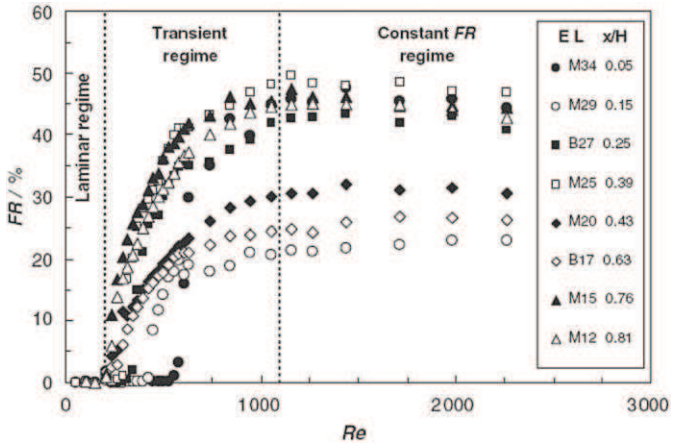

Fig. 10. Evolution of the fluctuation rates, *FR*, of the wall shear stress in a network of minichannels with the Reynolds number, *Re* (Huchet et al., 2007; reproduced with permission). The different measurement points are taken by individual probes at various axial positions, *x/H*, within the device.

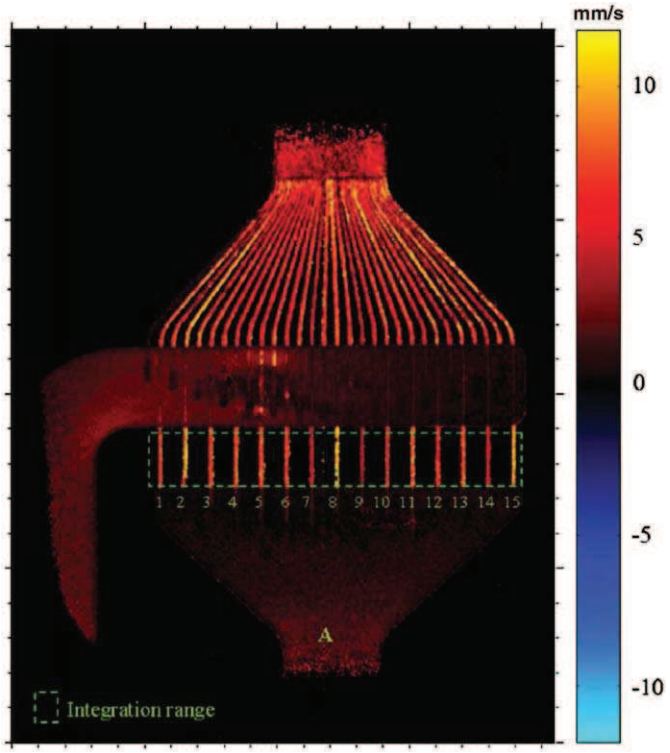

Fig. 11. Nuclear magnetic resonance velocity imaging in an interdigital micromixer (Ahola et al., 2006; reproduced with permission). The flow map is coloured by velocity magnitude (mm/s) and clearly identifies flow inhomogeneities across the channels. (For interpretation of the color bar legends in the figures, the reader is referred to the web version of this article.)

a short acquisition time (32 ms per velocity component measurement), which enables velocities of unsteady flows to be tracked accurately.

3. Gas–liquid dispersions

In this section, the experimental methods currently used for characterising the hydrodynamics and mixing in gas–liquid flows generated in microreactors are presented, as well as techniques for measuring the gas- and liquid-phase characteristics (e.g. bubble velocity and size, and liquid slug length).

3.1. Local hydrodynamics and mixing

Some of the techniques used for evaluating mixing and hydrodynamics in single phase flow in micro devices can also be employed for characterising gas–liquid flows. These methods enable a better understanding of mixing and flow phenomena, particularly in the liquid phase of the dispersion, which is necessary for the design and the enhanced performance of microreactors.

3.1.1. Dilution-based and reaction-based methods

Dilution-based and reaction-based experiments (Sections 2.1.1 and 2.1.2) can be applied to dispersed gas–liquid systems and offer qualitative information on mixing quality with similar technical limitations to the single phase experiments. Typically, measurements are made in the liquid phase of a gas–liquid slug flow. For this, two different but miscible liquid streams are first contacted together and then contacted with the gas phase to create the gas–liquid dispersion. For dilution-based methods, one of the liquid streams contains the tracer; for the reaction-based methods the liquid streams are constituted of the reactants. The evolution of the mixing of the tracer or the appearance of the reaction product is monitored in the same manner as for single phase mixing applications. The mixing is judged complete when the concentration of the dye or product is uniform within the liquid slug.

An example of applying a dilution-based method to study mixing in the liquid phase of a segmented gas–liquid flow is given by Günther et al. (2004). They used a fluorescent tracer (Rhodamine B) in ethanol to study mixing in the liquid phase of a gas–liquid dispersion in straight and meandering microchannels. Fig. 12 shows the instantaneous fluorescence images of Rhodamine B at different positions along the straight (left) and meandering (right) channels. The results show that the recirculation motion within the liquid segments enhances mixing between the two miscible liquid streams. Furthermore, the mixing in the liquid slug is faster in the meandering channel than in the straight geometry.

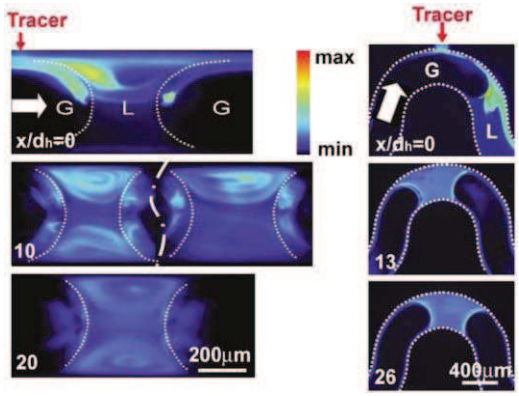

Fig. 12. Characterising mixing quality by the dilution of a fluorescent tracer in the liquid phase of a gas–liquid segmented flow in straight (left) and meandering (right) microchannels (Günther et al., 2004; reproduced with permission). Images depict instantaneous fluorescence fields at different hydraulic diameters down the microchannels. Fluid recirculation in the liquid slugs enhances mixing along the microchannel; fluid mixing is further enhanced in the meandering channel.

3.1.2. Micro particle image velocimetry

The application of μ-PIV to gas–liquid flows in micro devices is the same as that used for measuring single phase flow; however, generally the velocities in only one of the phases are determined. Typically, measurements are made in the liquid phase, which requires seeding with appropriate tracer particles. As in single phase experiments, this method enables the determination of instantaneous planar velocity fields comprising two in-plane velocity components. An additional difficulty of performing μ-PIV measurements in gas–liquid flow is the possible obtainment of spurious velocity vectors due to the gas bubbles and reflections at the gas–liquid interface. These artefacts can be removed by using filters specific to the seed tracer or in an image post-processing step.

There are several examples of the use of μ-PIV for measuring liquid flow in gas–liquid dispersions in microchannels. In addition to the dilution-based fluorescent tracer experiments described above, Günther et al. (2004) used μ-PIV to better understand flow and mixing improvement in the liquid slugs of segmented gas–liquid flow. Fig. 13(a) shows the instantaneous velocity fields and corresponding 2-dimensional streamlines in the liquid plug for the straight (left) and meandering (right) microchannel geometries. In both cases, there is recirculation motion within the liquid plug, which explains the enhancement of mixing in the liquid phase for these segmented flows. In addition, in the case of the straight channel the flow is composed of two symmetric but counter-rotating circulation loops, whereas the circulation loop in the case of the meandering channel is off-centred. This asymmetry of the flow pattern also explains the enhanced mixing performance in the meandering microchannel. Fries et al. (2008) have since shown that the asymmetric flow in liquid slugs in meandering channels depends on the channel dimensions, the radius of curvature, the turning angle, as well as the superficial velocities of the gas and liquid. They used μ-PIV not only to determine the flow patterns but also to calculate the 2-dimensional vorticity and swirling strength of the recirculation motion. Waelchli and von Rohr (2006) also used μ-PIV to investigate the effects of channel dimensions and the physico-chemical properties of the fluids on the recirculation of the liquid phase in gas–liquid flows in a straight microchannel. Fig. 13(b) shows the flow patterns within the liquid slug for water–nitrogen (left), water–ethanol (centre) and water–glycerol (right) flows. Their results suggest that the recirculation motion within the liquid phase is affected more so by the interfacial forces than the liquid viscosity. In fact, the interfacial tension between the gas and the liquid phases determines in part the shape of the leading and trailing edges of the bubbles, which affects the liquid recirculation.

μ-PIV can also be used to better understand the bubble formation process of gas–liquid flows in microchannels. Van Steijn et al. (2007) have shown with several planar μ-PIV measurements throughout the depth of a T-microchannel, that at no instant does the gas phase occupy the entire channel cross-section before bubble formation and that a significant amount of liquid flows over the forming bubble (Fig. 13(c)). By quantifying liquid flow rate passing over the forming bubble from the μ-PIV measurements, the bubble and liquid slug lengths to able to be correctly predicted. Xiong et al. (2007) have also used μ-PIV to investigate the effect of liquid flow on the bubble formation process in a co-flowing gas–liquid microreactor.

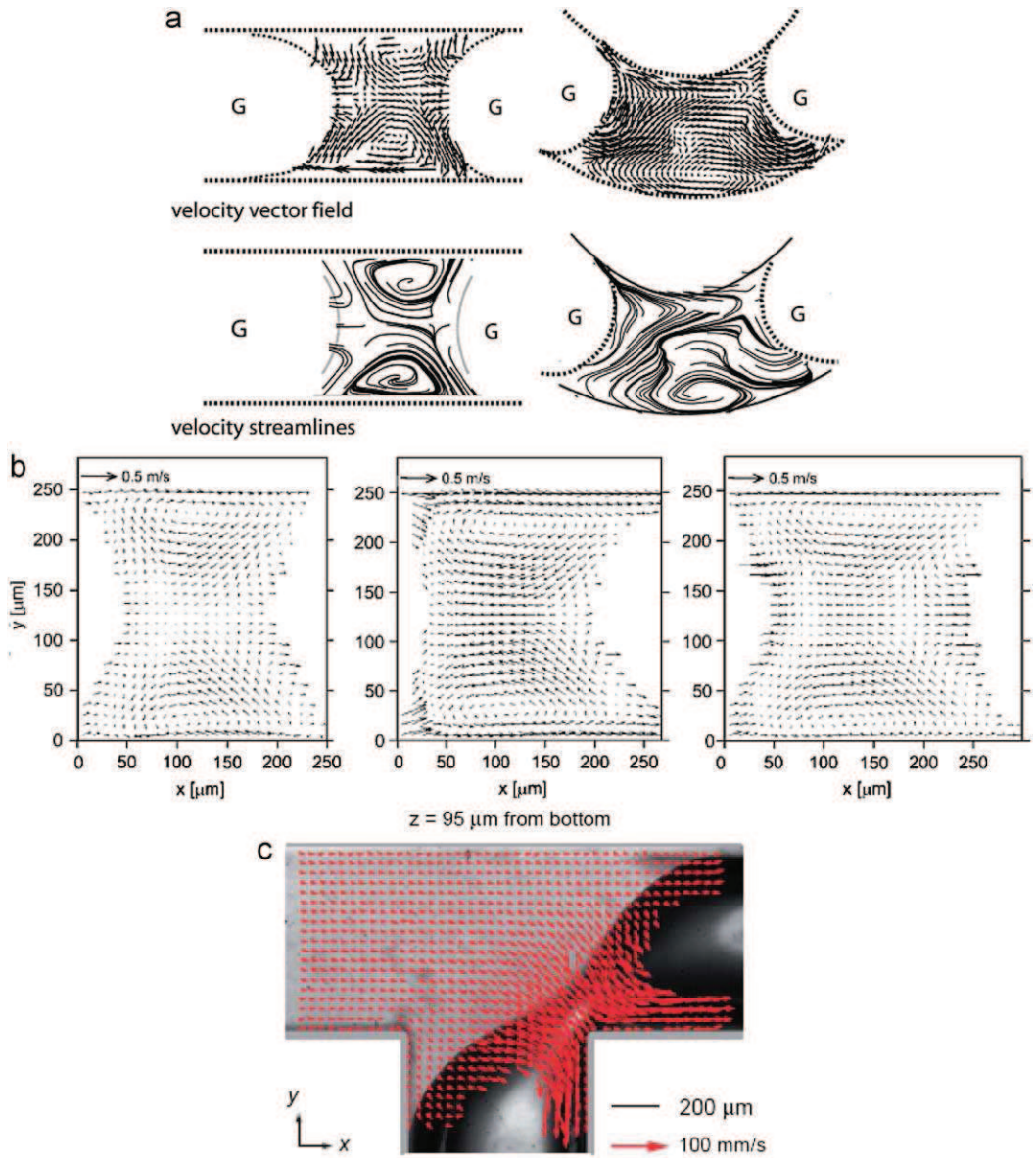

Fig. 13. Examples of liquid velocity fields measured by μ-PIV in gas–liquid flow in microchannels. (a) Comparison of vector fields and streamlines in the liquid plug of segmented flow in straight (left) and meandering (right) microchannels (Günther et al., 2004; reproduced with permission). (b) Flow patterns in the liquid slug of water–nitrogen (left), ethanol–nitrogen (centre) and glycerol–nitrogen (right) flows (Waelchli and von Rohr, 2006; reproduced with permission). The interfacial tension between the fluids modifies the shape of the bubbles, which affects the recirculation motion within the liquid phase. (c) Liquid flow patterns around a forming bubble in a T-microchannel (van Steijn et al., 2007; reproduced with permission). Quantification of the liquid flow rate passing over the forming bubbles from the velocity fields enables the prediction of bubble and liquid slug lengths.

3.2. Flow regimes and characteristics of the gas and liquid phases

Knowledge of the gas–liquid flow regime and the characteristics of the two phase flow are important for the performance of microreactors used for both physical and chemical transformations. For chemical reactions, the characteristics of the gas–liquid flow determine the specific interfacial area between phases and the mass transfer efficiency. For physical transformations, such as the generation of foams, the stability and the physical attributes of the dispersion depend on the structure and characteristics of the two-phase flow. To identify flow regimes and the characteristics of the gas and liquid phases in micro devices, classical microscopy imaging techniques are typically used; however, some other non-intrusive sensors have also been developed. The experimental techniques described below typically give information on the scale of segregation between the gas and liquid phases.

3.2.1. Imaging techniques

Flow imaging using a digital camera coupled with a lens or a light microscope for magnification is the most often used technique to characterise gas–liquid flow in micro devices. This method provides qualitative information about gas–liquid flow patterns in micro devices and gives access to quantitative information on the individual phases, including bubble frequency, size and velocities, and liquid slug lengths (when applicable). The set-up for gas–liquid flow visualisation using such imaging techniques is straight forward and the only essential requirement is direct optical access to the micro channel flow. Limitations do exist when applying the method to multi-layered channel networks since flow visualisation is conducted perpendicular to the device. This limitation restricts flow visualisation to the first layer of channels only. The specifications of the microscope and the camera used depend largely on the type and resolution of the

information required. For sharp definition of the gas–liquid interface, high magnification and high resolution cameras with sufficiently short shutter times are recommended. For recording fast transient events, such as bubble formation or break up, high speed digital cameras that enable the acquisition of up to several thousand frames per second are usually needed.

There are a large number of studies in the literature that employ visualisation techniques for characterising gas–liquid flows in microchannels and other miniaturised devices. For illustrative purposes and to guide the reader to some initial literature, a selection of these studies and the information acquired is listed in Table 2. From this it is apparent that a simple set-up of a digital camera and magnification system (microscope or objective) is sufficient to visualise gas–liquid flow regimes and bubble sizes in microchannels. However, if information of a more precise nature (e.g. bubble breakup, velocities and frequencies) is required, a high speed camera is needed to capture the transient phenomena. Some example images of gas–liquid flow obtained by different imaging systems are shown in Fig. 14. Fig. 14(a) shows gas–liquid flow regimes visualised using a digital camera and a stereomicroscope (Haverkamp et al., 2006). The stereomicroscope has the quality of a large working distance and depth of field, as well as 3-dimensional viewing. Although the different flow regimes can be seen the contrast between phases is rather poor; this highlights the importance of lighting when visualising flows in microchannels. Waelchli and von Rohr (2006) used fluorescent rhodamine in the liquid phase and laser light to increase the contrast between the gas and the liquid phases, as shown in Fig. 14(b). The distinction between phases is clear, the gas phase being shown by dark areas. Fig. 14(c) shows bubble breakup visualised with a high speed camera (1000 fps). Of course, this transient behaviour can only be captured using a camera with a higher frequency than the phenomenon itself. Although fluorescence has not been used here, the contrast between phases is very good, which is possible with appropriate lighting.

3.2.2. Methods using non-intrusive sensors

Flow imaging using digital cameras and microscopes typically requires a significant financial investment since the equipment is relatively expensive. Its application is also limited to transparent micro devices and single layer channel networks. In response to some of these limitations, there has been some interest in the development of non-intrusive sensors that can be integrated into micro devices relatively simply and cheaply, while allowing sufficient flow monitoring and characterisation.

Wolffenbuttel et al. (2002) have used infrared absorption sensors at two streamwise positions in small size glass capillary tubes to discriminate between phases in gas–liquid slug flow. This low-cost measurement method, which is simple to use, enables determination of the bubble and liquid slug lengths, as well as the velocities, with sufficient resolution. Another recently developed non-intrusive sensor for gas–liquid flows is that based on the total internal reflection of light at the gas–liquid interface (Kraus et al., 2004). This integrated velocimetry technique employs pairs of sensors to characterise the gas–liquid flow distribution and to measure gas and liquid slug lengths, gas-slug frequencies and velocities. Although this method relies on laser light, the integration of waveguided optical flow sensors has the advantage of enabling the measurement and characterisation of gas–liquid flow in channels within a multilayer microchannel network and not just the top layer of channels (de Mas et al., 2005). Leung et al. (2004) report on continuous real-time bubble monitoring in microchannels using a method based on refractive index detection. A laser beam is directed to the gas–liquid flow in the

Table 2
Examples of the information that can be obtained on gas–liquid flow in microdevices with various imaging systems.

Reference	Imaging system	Information obtained
Waelchli and von Rohr (2006)	Digital camera with microscope (spatial resolution of 0.99 μm). Lighting with laser. Rhodamine B was added to the liquid phase to improve contrast between gas and liquid phases.	Gas–liquid flow patterns
Van Steijn et al. (2007)	High speed camera.	Bubble formation Interface shape Bubble and liquid slug lengths Bubble velocity
Xiong et al. (2007)	High speed camera (8000 fps, shutter speed 125 μs) with microscope. Used at 500 fps.	Bubble formation Bubble size and distribution Bubble frequencies
Salman et al. (2006)	High speed camera with a 40 × lens. Used at 125 and 250 fps.	Duration and mechanism of Taylor bubble formation.
Haverkamp et al. (2006)	Digital camera with stereomicroscope. High speed camera with microscope (10 000 fps, shutter speed 12 μs).	Gas–liquid flow patterns Bubble size distributions
Cubaud et al. (2006)	High speed camera (10 000 fps) with microscope or lens.	Gas–liquid flow patters (dry and wet foams)
Yue et al. (2007)	High speed camera.	Gas–liquid flow patterns
Yu et al. (2007)	High speed camera (1000 fps) with a 4 × microscope objective.	Bubble formation in the bubbly and slug flow regimes Bubble size and shape
Warnier et al. (2008)	High speed camera (10 000 fps, shutter speed 12 μs) with microscope (spatial resolution of 3.6 μm).	Bubble and liquid slug lengths Bubble velocity Bubble frequency
Kristal et al. (2008), Kristal (2008)	Digital camera.	Bubble size distribution in an electrochemical microreactor with a gas-evolving reaction

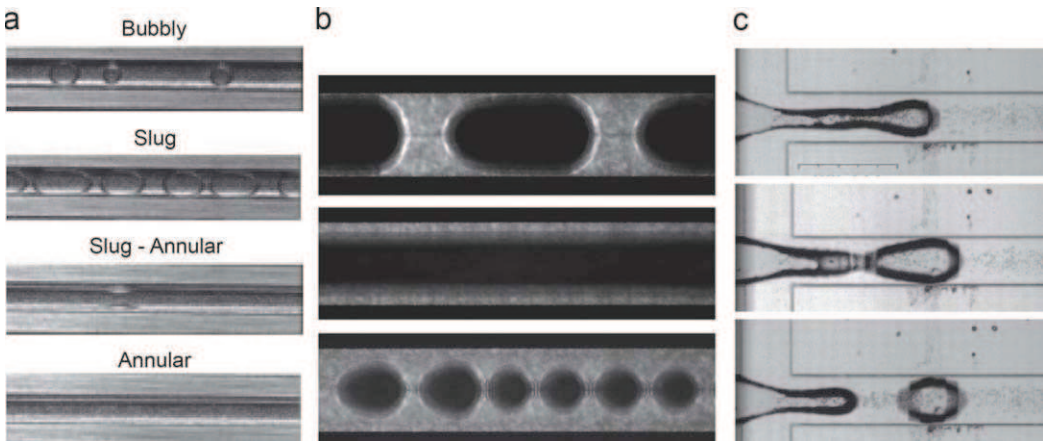

Fig. 14. Examples of gas–liquid flow imaging. (a) Nitrogen–isopropanol dispersion in one 1100 μm × 170 μm channel of a microbubble column composed of 64 parallel channels. Images are obtained with a stereomicroscope and a CCD camera (Haverkamp et al., 2006; reproduced with permission). (b) Nitrogen-water flow patterns visualised using Laser Induced Fluorescence and captured with a digital camera coupled with a microscope (Waelchli and von Rohr, 2006; reproduced with permission). The laser light is used to excite Rhodamine B in the liquid phase, which is visualised as the light grey areas in the images. (c) The formation of air bubbles in a sugar solution flowing in a 250 μm channel is captured with a high speed camera (1000 fps) and a microscope with a 4 × objective (Yu et al., 2007; reproduced with permission).

microchannel and as it passes through the flow, it is refracted to varying degrees depending on the medium (i.e. gas or liquid) it is passing. The refracted light is collected by a position sensitive detector, which registers a voltage signal. This simple and cost-effective technique for monitoring bubbles in micro devices, which requires direct optical access to the flow, enables information on the size and frequency of bubbles to be obtained. Another optical method to characterise bubbles and gas–liquid flow regimes has been described by Revellin et al. (2006, 2008). They use two laser beams and photodiodes positioned at two streamwise locations to measure the variation of the light intensity as the gas and liquid phases move through the microchannel. The resulting voltage signal from the photodiodes is measured at a rate of 10 000 measurements/s. From these measurements, the gas–liquid flow regime (bubbly flow, slug flow, semi-annular flow and annular flow) can be identified, in addition to the bubble frequency and length.

4. Liquid–liquid dispersions

4.1. Hydrodynamics and mixing

As for dispersed gas–liquid flows, accurate measurements and visualization of the flow and mixing in liquid–liquid dispersion are important for understanding the physical phenomena and to improve process performance. Again, some of the techniques developed for single phase flow characterisation can also be applied to liquid–liquid flow.

4.1.1. Dilution- and reaction-based methods, and concentration profiling

The dilution- and reaction-based experiments described in Sections 2.1.1 and 2.1.2 can also be conducted in liquid–liquid systems. Typically, these experiments are carried out in the dispersed phase (i.e. within the droplet) of a liquid–liquid flow. However, characterisation of mixing in the continuous liquid phase is also possible, in a manner similar to that described for gas–liquid flows (Section 3.1.1). In both cases, two different but miscible liquid streams are first contacted—one stream containing a tracer, or alternatively each stream containing reactants. These are then contacted with an immiscible liquid stream. Mixing is assessed in a similar way to the single phase systems.

Fig. 15 presents selected examples of studies that have investigated mixing within droplets in liquid–liquid flows in micro channels. Tice et al. (2003) compare two dilution-based methods to study mixing within droplets generated in microchannels. The first dye system involves concentrated organic food dyes. Fig. 15(a) shows the formation of droplets with red and green coloured aqueous streams and water. The authors found that the highly concentrated organic dyes affect the interfacial properties of the aqueous phase, which leads to modification of flow patterns within the drop, the drop shape and therefore mixing. To observe mixing within the droplets without modifying the interfacial properties, an aqueous solution of $Fe(SCN)_x^{(3-x)+}$ complex, which is red in colour, was diluted with colourless water streams. Fig. 15(b) shows the effect on mixing of the position of the tracer injection in the drop formation process. The switching of the position of the coloured stream leads to the formation of drops with complementary dye distributions, and was shown to affect the evolution of mixing within the drop along the channel. In a second study, Tice et al. (2004) used the same inorganic complex $Fe(SCN)_x^{(3-x)+}$ to investigate the effect of contacting streams with different viscosities on mixing. The upper images in Fig. 15(c) show the mixing behaviour within the drop when all three drop reagents are non-viscous and have the same viscosity. In the lower images, a dyed viscous aqueous stream is injected in the left most inlet and contacted with two non-viscous streams to form the droplets. By monitoring the dilution of the organic dye within the drops, it was observed that aqueous reagents of differing viscosities may mix more rapidly than aqueous reagents with match viscosities. Fig. 15(d) shows mixing in aqueous droplets using xylene cyanol dye (Sarrazin et al., 2007). The strong contrast between the dyed and the undyed reagents facilitates the image analysis procedure, which enables mixing time to be determined from grey scale levels in the images. Sarrazin et al. (2007) have also employed an acid-base reaction to study mixing in droplets, whereby a sodium hydroxide solution coloured with bromothymol blue indicator is contacted with hydrochloric acid. This reaction is instantaneous, resulting in the bleaching of the blue indicator to yellow, and allows the poorly mixed zones within the drop to be identified, as indicated in Fig. 15(e). Wang et al. (2007) have used a fluorescent dye to follow the mixing of between two coalescing water droplets. Fluorescein disodium salt was added to one aqueous phase before coalescence with the other aqueous phase and the dilution of the tracer was followed using a CCD camera (30 Hz). In order to obtain

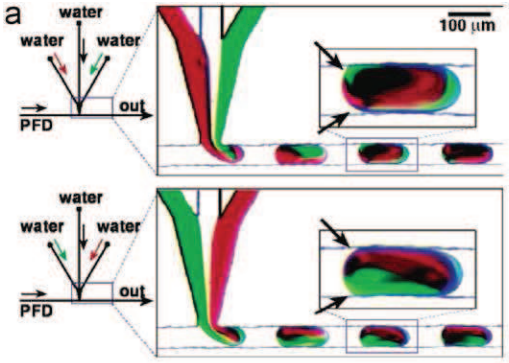
a
water
water
water
out
PFD
100 μm

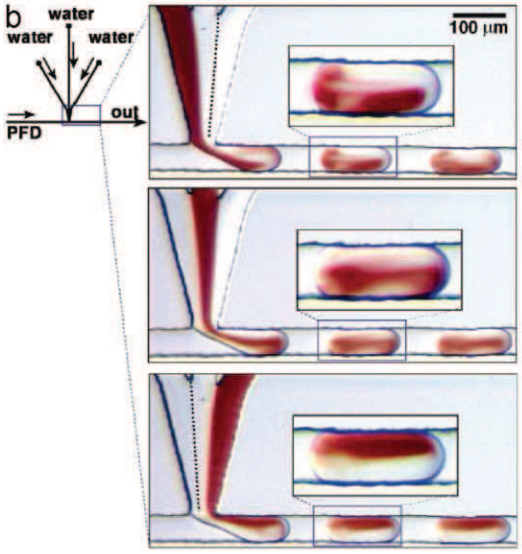
b
water
water
water
out
PFD
100 μm

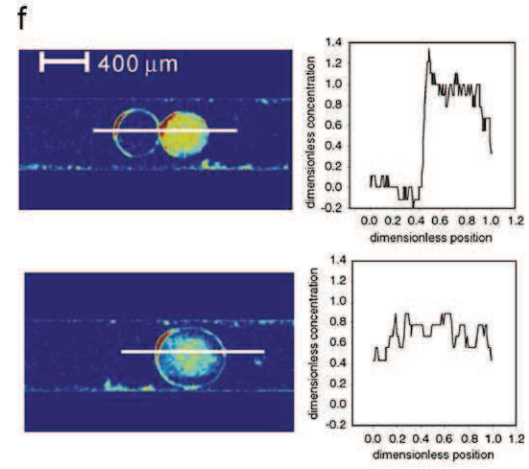
f
400 μm
dimensionless concentration
dimensionless position

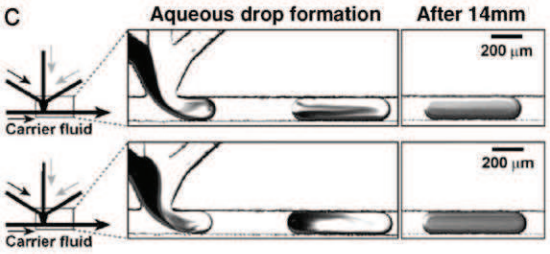
c
Aqueous drop formation
After 14mm
Carrier fluid
200 μm

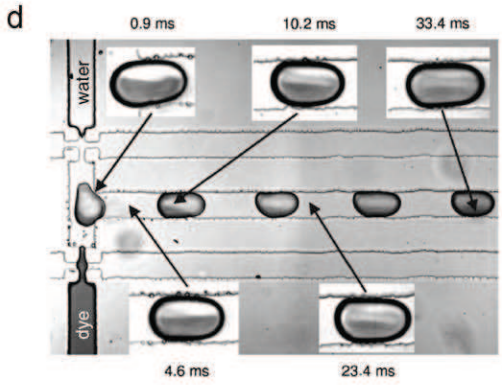
d
0.9 ms
10.2 ms
33.4 ms
water
dye
4.6 ms
23.4 ms

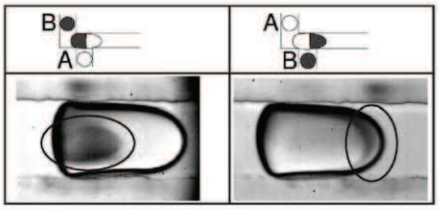
e
B
A
A
B

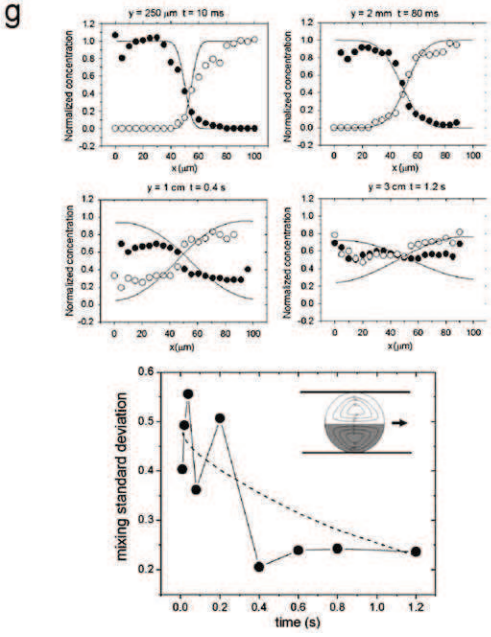
g
y = 250 μm t = 10 ms
y = 2 mm t = 80 ms
y = 1 cm t = 0.4 s
y = 3 cm t = 1.2 s
Normalized concentration
x (μm)
mixing standard deviation
time (s)

qualitative information on the progression of mixing of fluorescein between the coalescing drops, a concentration profile across the coalescing drops was determined, as shown in Fig. 15(f). This approach provides information on the global length scales of mixing at the scale of the drop. It is clear from the graphs shown Fig. 15(f) how the pixel size of the images is important for the spatial resolution of the mixing quality. Fig. 15(g) shows concentration profiles measured using scanning confocal Raman microspectroscopy within dispersed aqueous droplets (Cristobal et al., 2006). For these measurements, the sampling volume was a very small cylinder with a diameter of 5 μm and a height of 15 μm. As a result, the line scans made are highly resolved and very close to a true 1-dimensional transect with zero thickness. For the results shown in Fig. 15(g), the Raman signals have been averaged over 350 droplets, as well as continuous phase slugs. With respect to this averaging procedure, the authors point out the importance of identifying the individual signals scattered by the aqueous droplets and the continuous oil phase from the total scattered signal. The authors also address the modification of the concentration profile by the curvature of the droplets and suggest a normalisation procedure to obtain the concentration profiles within the droplets (Fig. 15(g)), hence allowing the temporal evolution of the state of mixing in the droplets to be followed.

4.1.2. Micro particle image velocimetry

The measurement of velocity fields in liquid–liquid dispersions in micro devices is possible using the μ-PIV technique, as described in Section 2.2.1. Typically, in the application of μ-PIV to liquid–liquid flows, the hydrodynamics of only one phase is studied at a time. Most often, the velocity fields in the dispersed phase (i.e. the droplets) have been measured. These measurements generally provide instantaneous planar velocity fields comprising two-in plane velocity components. However, extension of the technique with confocal microscopy enables 3-dimensional, three component velocity fields to be obtained. In addition to the usual technical requirements (e.g. optical access to the flow, seeding), the application of μ-PIV to liquid–liquid flows requires the matching of refractive indices of the working fluids and the channel material to be matched in order to minimize the refraction of light at the liquid–liquid and liquid–solid interfaces.

Several studies in the literature report the use of μ-PIV to measure the velocity fields within droplets and/or the surrounding liquid. Fig. 16 shows some selected results from a range of studies reported in the literature. Fig. 16(a) shows the relative velocity fields at different horizontal cross-sections in an aqueous droplet suspended in silicon oil in a microchannel of width 60 μm and depth 50 μm (Sarrazin et al., 2006). The measurements have been taken with a 20× objective with a numerical aperture of 0.5; this gives a resolution in the depth-wise direction of ~9 μm, thus allowing several velocity fields to be measured within the droplet. King et al. (2007) have used μ-PIV to investigate the effects of bulk fluid velocity and droplet size on the recirculation patterns within droplet in a microchannel. They found that the velocity profile in the droplets tended towards a flat zero-gradient profile for lower velocities and shorter drops, therefore hindering the recirculation within (Fig. 16(b)). Fig. 16(c) shows 3-dimensional maps of the three relative velocity components within an aqueous drop in a microchannel obtained using high-speed confocal μ-PIV (Kinoshita et al., 2007). This measurement system allows planar images to be obtained at a frequency of 2000 frames/s and a depth-wise resolution of 1.88 μm. The measurements directly provide 3-dimensional 2-component velocity fields, however, the high resolution in the vertical direction enables the third velocity component to be calculated using the measured velocity data and the equation of continuity. Wang et al. (2007) have measured the velocity fields within aqueous droplets moving in high aspect ratio microchannels (1000 μm × 100 μm). Fig. 16(d) shows the image of the tracer particles in the droplet (left), as well as the absolute (centre) and the relative (right) velocity fields in the droplet. Their results show that the recirculation field within the droplet depends on the droplet size relative to the width of the microchannel. Fig. 16(e) shows the velocity fields within (left) and around (right) a silicon oil droplet forming in an aqueous cross-flow (Timgren et al., 2008). The μ-PIV measurements, performed by seeding either the continuous or dispersed phase, have allowed the hydrodynamics of drop formation and shear-stress levels at the liquid–liquid interface to be determined, which are crucial for understanding the physical drop formation process.

4.2. Drop characterisation

Characterisation of the length scales of liquid–liquid dispersions via determination of the drop size and the drop size distribution is important for evaluating the performance of liquid–liquid mixing and dispersion processes in microchannels and microreactors. In particular, the characteristics of the droplet population are necessary as they are directly linked to the physical quality of the dispersion (e.g. product stability, controlled product properties), as well as the performance of transport and reaction processes.

The techniques described below are known methods for the characterisation of emulsions, and not restricted to emulsions generated in micro devices. Since emulsions typically have a small characteristic size regardless of the processing equipment used, and that characterisation is most often carried out off-line on small samples, most of the known conventional characterisation methods are applicable to emulsions generated in micro devices. Nevertheless, many of the techniques have not yet been employed for characterising microchannel dispersions. The following paragraphs detail the various techniques available for characterising emulsions and drop size, and provide the main requirements, limitations and associated difficulties of each technique. In addition, Table 3 provides a summary of the main characteristics, advantages and

Fig. 15. Examples of the application of dilution-type and reaction-type experiments for studying mixing within droplets. (a) Observation of mixing in aqueous droplets using concentrated organic food dyes; all organic dyes were found to affect the interfacial properties of the drops, modifying drop shape and mixing within (Tice et al., 2003; reproduced with permission). (b) Effect of switching the injection position of the red aqueous solution ($Fe(SCN)_x^{(3-x)+}$ complex) with respect to two colourless aqueous streams of KNO_3 on the mixing within droplets (Tice et al., 2003; reproduced with permission). (c) Dilution of a red (dark) aqueous solution ($Fe(SCN)_x^{(3-x)+}$ complex) to study the effect of viscous fluids on mixing in aqueous drops; all three aqueous streams are non-viscous with $\mu \approx 2$ mPa s (top); the dark stream is viscous ($\mu \approx 18$ mPa s) and colourless streams are non-viscous ($\mu \approx 2$ mPa s) (bottom) (Tice et al., 2004; reproduced with permission). (d) Mixing of water and a dark dye (xylene cyanol) in droplets carried in a continuous phase of silicone oil (Sarrazin et al., 2007; reproduced with permission). (e) Evolution of mixing in aqueous drops using an instantaneous acid–base reaction and bromothymol blue indicator (Sarrazin et al., 2007; reproduced with permission). (f) Dilution of a fluorescent tracer in aqueous droplets and corresponding concentration profiles at coalescence (left) and some time after coalescence (right) (Wang et al., 2007; reproduced with permission). (g) Evolution of concentration profiles of $K_4Fe(CN)_6$ (●) and $K_3Fe(CN)_6$ (○) solutions in dispersed droplets along a microchannel (top four images) (Cristobal et al., 2006; reproduced with permission). The species concentration is measured by confocal Raman microspectroscopy along a transect within the droplet. Mixing performance is evaluated by following the standard deviation of the species concentration about the mean value along the length of the microchannel. (For interpretation of the references to color in this figure legend, the reader is referred to the web version of this article.)

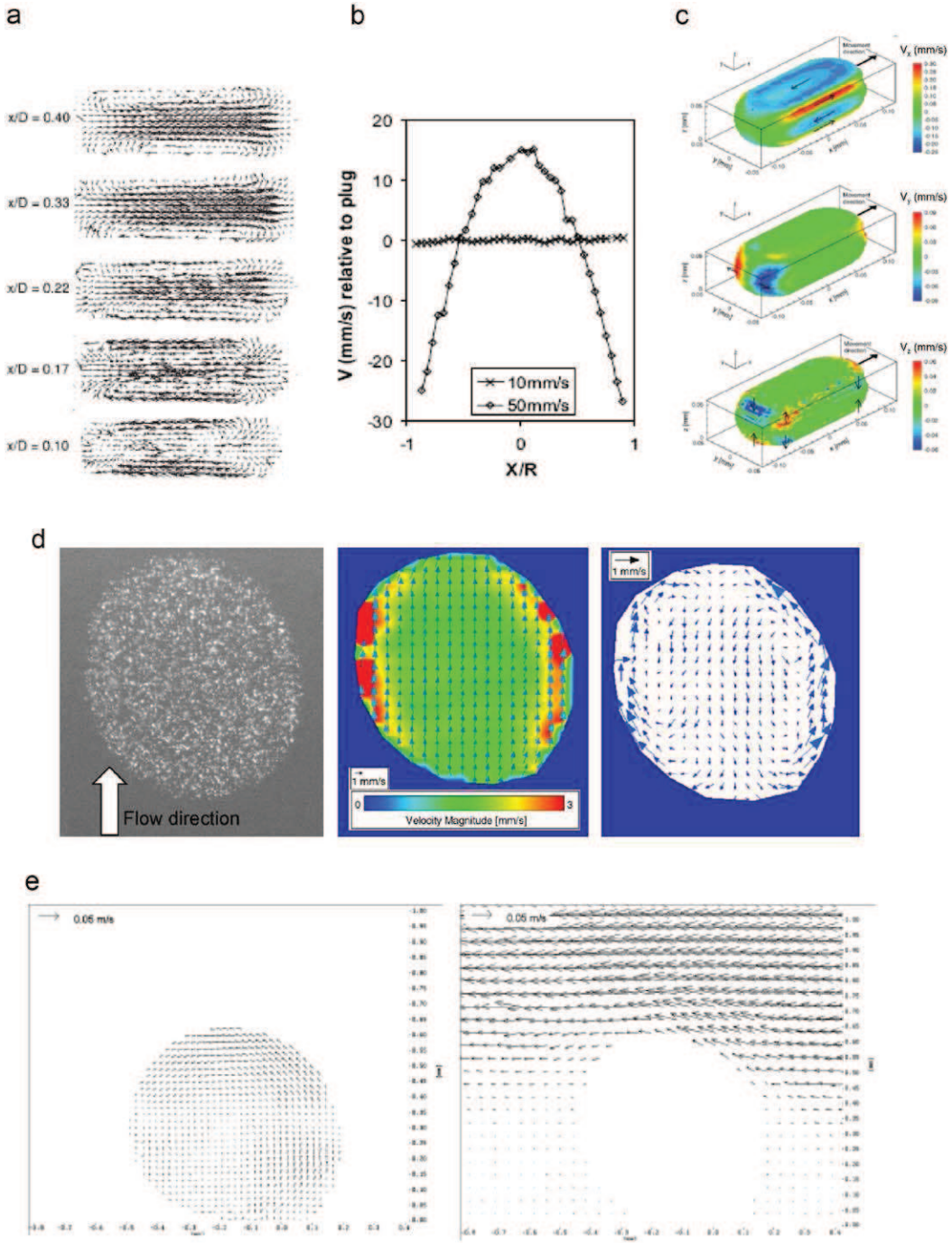

Fig. 16. Examples of μ-PIV measurements in liquid–liquid systems. (a) Velocity fields in the reference frame of the droplet taken at different heights in the droplet; x/D=0.42 corresponds to the horizontal centre-line of the drop; x/D=0 is in line with the microchannel wall (Sarrazin et al., 2006; reproduced with permission). (b) Relative velocity profiles within an aqueous drop of length of 2.5 mm for bulk mean velocities of 10 and 50 mm/s (King et al., 2007; reproduced with permission). (c) Three-dimensional views of the relative velocity components inside a moving droplet measured using confocal micro PIV: V_x (top); V_y (centre); V_z (bottom) (Kinoshita et al., 2007; reproduced with permission). (d) μ-PIV measurement of the velocity field inside an aqueous moving droplet (channel size=100 m × 1000 m, total flow rate=1100 L/h, flow rate ratio=10:1. (Left) Digital image of particles. (Centre) Absolute velocity field. (Right) Velocity field relative to the drop reference frame (Wang et al., 2007; reproduced with permission). (e) Velocity fields within (left) and around (right) a silicon oil droplet forming in an aqueous cross flow of 0.11 m/s (Timgren et al., 2008; reproduced with

limitations of the methods, enabling rapid comparison between them.

4.2.1. Microscopy

Microscopic techniques are able to provide information about structure, dimensions, and organization of the components within liquid–liquid dispersions. In the forthcoming paragraphs, the microscopic methods that are most extensively used for the examination of the different levels and types of structural organization of liquid–liquid dispersions are detailed.

4.2.1.1. Conventional optical microscopy. Conventional optical or light microscopy has been widely applied to characterise emulsions, and in particular, their droplet size distribution. In light

Table 3
Summary of resulting information, advantages and limitations of experimental methods for determining the characteristics of liquid–liquid dispersions and emulsions.

Characterisation method	Resulting information	Resolution of measurement	Advantages/limitations/associated difficulties
Microscopy	Information on structure and organisation of phases within liquid–liquid dispersions, as well as droplet dimensions		
Optical microscopy		Down to 200–500 nm	Typically does not require sample preparation Can be coupled with high speed camera for monitoring drop formation processes
Confocal scanning laser microscopy (CSLM)	Three-dimensional imaging	Down to 200 nm in focal plane and 500–800 nm along optical axis	Staining of one phase using fluorescent compounds or dyes for improved contrast
Transmission electron microscopy (TEM)	Two-dimensional image of the internal structure of emulsion	0.2–1 nm	Sample preparation difficult Sample must be extremely thin (0.05–0.1 nm)
Scanning electron microscopy (SEM)	Three-dimensional image of the topography of the emulsion	3–6 nm	Sample preparation difficult but easier than TEM Does not require ultra thin samples
Atomic force microscopy (AFM)	Three-dimensional imaging of surfaces	Lateral resolution ~nm Axial resolution ~tens of nm	Small scan size (a few micrometers) Imaging requires long scanning time
Static light scattering	Drop size distribution and concentration	Drop diameters of 0.2–2000 μm	Dispersed phase fraction < 0.1 wt% Dilution of sample often required Equipment with flow through cells available for on-line measurements
Dynamic light scattering	Drop size and distribution	Drop diameters of 3 nm–5 μm	Dispersed phase fraction < 0.1 wt% in transmission mode Dispersed phase fraction < 10 wt% in backscattering mode
Diffusing wave spectroscopy	Information on local dynamics of liquid–liquid dispersion (drop size, interactions between droplets, interface properties, changes in continuous phase rheology …)		No restrictions on dispersed phase concentration
Electric pulse counting	Drop size distribution	Drop diameters of 0.4–1200 μm	Dispersed phase fraction < 0.1 wt% Dilution of sample often required Droplets must be suspended in electrolyte solution for accurate measurements
Ultrasonic spectroscopy	Drop size, distribution and concentration	Drop diameters of 0.01–1000 μm	Suitable for high and low concentrated dispersions (> 40% and ~0.1% dispersed phase volume fraction, respectively) Ultrasounds are non-destructive, non-intrusive and transparent to most materials and therefore the method is particularly suitable for on-line measurements
Nuclear magnetic resonance	Drop size distribution	Drop diameters of 0.2–100 μm	Small sample (~0.5 g) without any preparation Suitable for measurements of transparent and opaque dispersions in optically opaque systems *In-situ* measurements possible
Electroacoustics	Drop size distribution and zeta potential (related to the electrical charge of the drop)	Drop diameters of 0.1–10 μm	Suitable for concentrated dispersions (up to 40% dispersed phase volume fraction) No dilution of sample required Drops must be electrically charged and have a significant density difference to the continuous phase

microscopy, the magnified images are formed by means of a light or photon beam focused by glass lenses. Considering this, the resolution of an optical microscope, i.e. the shortest distance between two points on a specimen that can still be distinguished by the observer or camera system as separate entities, depends basically on the objective numerical aperture and the wavelength spectrum of light used to image a specimen. Under optimal conditions, resolution may range between 200 and 500 nm. Therefore, conventional optical microscopy has limited application since many emulsions, like mini- and micro-emulsions, contain structures below the lower limit of resolution (Aguilera and Stanley, 1999). Although imaging an emulsion with light microscopy does not require any sample preparation, the poor contrast between the phases in emulsions makes it difficult to reliably distinguish the phases from each other using conventional bright-field optical microscopy. Contrast can be improved by chemically staining one

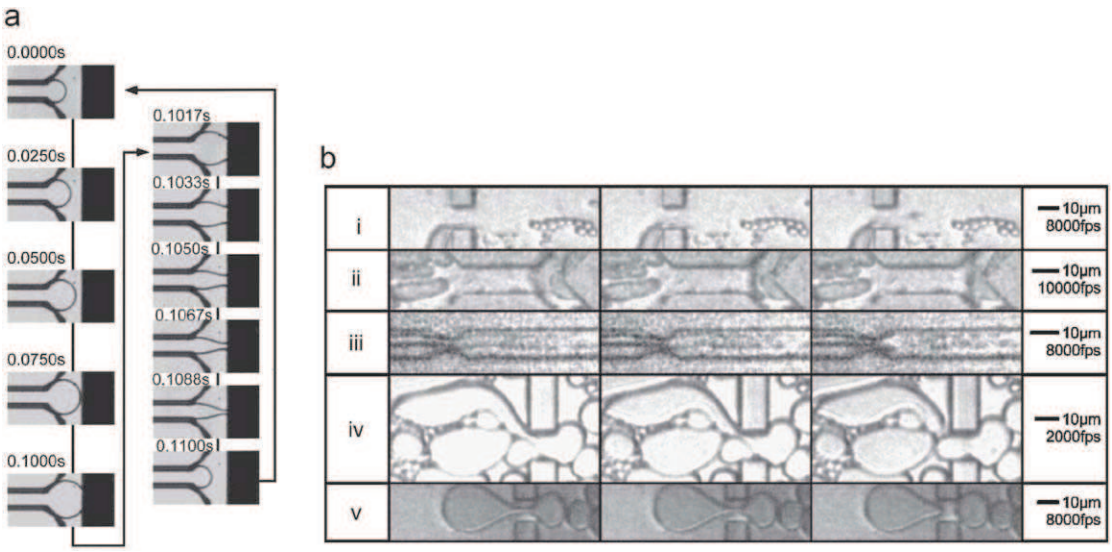

Fig. 17. Examples of images obtained using a microscope coupled with a high speed camera for monitoring drop formation in micro devices. (a) Time evolution of triolein droplet formation in water within a microchannel (Sugiura et al., 2001; reproduced with permission) (b) Different drop formation processes of *n*-hexadecane drops in water; flow from left to right (van der Zwan et al., 2006; reproduced with permission); (i) snap-off due to localized shear forces; (ii) snap-off due to localized shear forces; (iii) break-up due to interfacial tension effects—Rayleigh instability; (iv) break-up due to steric hindrance between droplets; (v) break-up due to interfacial tension effects—Laplace instabilities.

phase of the emulsions or by modifying the design of the optical microscope; for instance, phase contrast or differential interference contrast microscopes are means to overcome limitations related to contrast (Murphy, 2001).

Conventional optical microscopy, however, can provide valuable information about the size distribution of emulsions containing large droplets and enables the visualisation of flocculation and coalescence phenomena (Mikula, 1992), which may control emulsion stability. Nowadays, with the coupling of optical microscopes and high speed digital cameras, the use of conventional light microscopy has opened new applications, such as the monitoring of droplet-formation during the emulsification process—for instance during micro-channel emulsification as shown in Fig. 17 (Sugiura et al., 2001; van der Zwan et al., 2006)—and rheo-optics, which combines optical microscopy and mechanical tests for analysing the breakdown of flocculated droplets in shear fields (van der Linden et al., 2003).

4.2.1.2. Confocal scanning laser microscopy (CSLM). CSLM is an optical microscopic technique that was commercially developed in the early nineties and has several advantages over conventional optical microscopy and electron microscopy. Illumination is achieved by scanning one or more focused beams of light, usually from a laser, across the specimen. This point of illumination is brought to focus in the specimen by the objective lens, and laterally scanned using some form of scanning device under computer control. The sequences of points of light from the specimen are detected by a photomultiplier tube through a pinhole, and the output from the photomultiplier is built into an image and displayed by the computer (Ferrando and Spiess, 2000).

CSLM can be used in transmission and reflection modes, but fluorescence imaging proves to be the most powerful technique when applied to emulsions. One of the main advantages of the confocal microscope is the exclusion of out-of-focus blur. The fluorescence emissions from the illuminated regions of the specimen above and below the in-focus point are not allowed to reach the photomultiplier, as a pinhole in front of the detector ensures that only light from the in-focus point is collected. This is clearly seen in Fig. 18(a), which shows a planar section of an oil-in-water emulsion. Different focus levels make optical sectioning possible and a thick specimen can be imaged in three dimensions; this is one of the most useful properties of CSLM. By combining the information on several focal planes that is on optical slices stored in a computer, a 3-dimensional image that describes the object can be reconstructed as shown in Fig. 18(b).

As in conventional optical microscopy, the limits of CSLM are related to the resolution of measurement. Resolution in CSLM is primarily a function of the numerical aperture of the optical system and the wavelength of the light, but it can be also limited if the signal levels represent so few quanta that the signal lacks the statistical precision to produce a 'visible' feature or if the data is not correctly sampled because the pixels are two large. In the best cases, the CSLM resolves 200 nm in the focal plane (x,y) and only 500–800 nm along the optical axis (z).

To improve the visualization of the emulsion structure, the natural auto-fluorescence of certain compounds, fluorescent chromophores that bind selectively to specific components (e.g., proteins, fat, or carbohydrates) or fluorescent dyes that are more soluble in one phase than the other (e.g., oil vs. water) are used to prepare the emulsions.

CSLM can be employed for the determination of droplet size distributions (van Dalen, 2002), but it also enables the characterisation of emulsion stability by monitoring droplet creaming and flocculation (Dickinson et al., 2003) or by following changes in interfacial composition on emulsion droplets (Heertje et al., 1996). CSLM has also been used, although not in microchannels, to study the structural organization of concentrated emulsions and the droplet interactions within (Brujic et al., 2003a, b), as well as for the characterisation of double emulsions (Koo et al., 2006). Guillot and Colin (2005) have used CLSM and high speed imaging to visualise the formation of droplets in a T-junction microchannel. The CLSM has enabled the 3-dimensional structure of the flow to be observed in real-time, and therefore provided insight into the blocking-pinching mechanism responsible for drop formation.

4.2.1.3. Electron microscopy. Electron microscopy includes several available electronic microscopy techniques, such as TEM

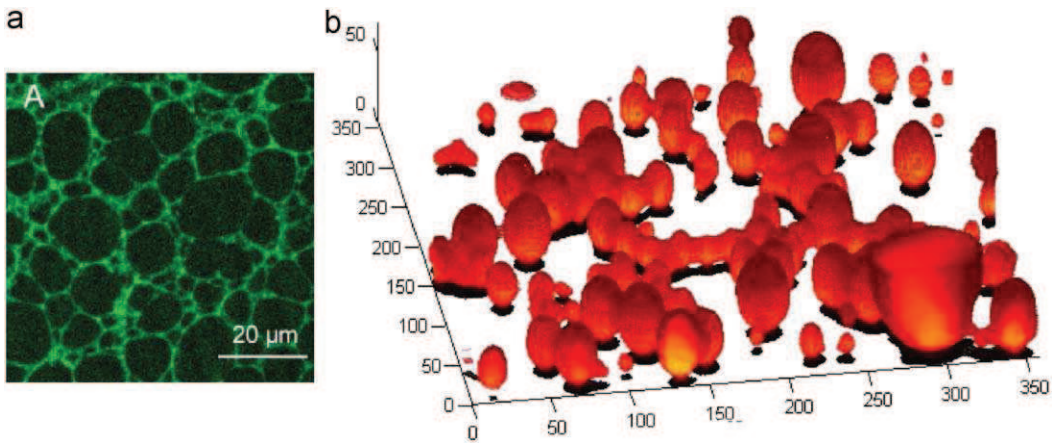

Fig. 18. Examples of CSLM images of liquid–liquid dispersions. (a) Two-dimensional CSLM micrograph of an oil-in-water emulsion containing 75 wt% oil (Romero et al., 2008; reproduced with permission). (b) Three-dimensional reconstruction of CSLM micrographs of an oil-in-water emulsion obtained by Premix membrane emulsification with Tween20 2% as emulsifier. *X*, *Y* and *Z* axes in pixels (*X*pixel size=*Y*pixel size=0.25 µm; *Z*pixel size=0.3 µm).

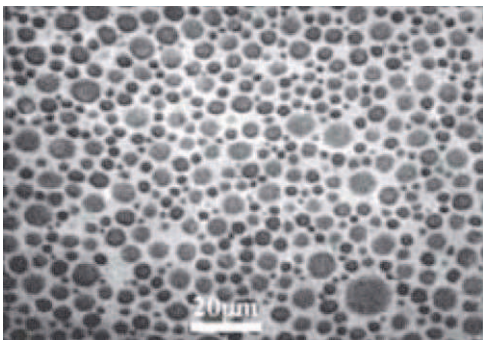

Fig. 19. Example of an oil-in-water emulsion imaged by ESEM (Stokes et al., 1998; reproduced with permission). The droplets of oil (dark regions) are clearly seen in the continuous phase of water (light regions).

(transmission electron microscopy) and SEM (scanning electron microscopy). Electron microscopes form the image using an electron beam for the illumination source, which is focused by magnetic lenses. In principle, the smallest size that can be resolved by electron microscopy is about 0.2 nm, however, in practice it is usually about 1 nm due to limitations in the stability and performance of the magnetic lenses. SEM and TEM differ essentially in the method of image formation; SEM is used to examine surfaces from which a 3-dimensional image of the topography of the specimen is produced, whereas TEM visualises the internal structure of the specimen by producing a 2-dimensional image of a thin slice (Aguilera and Stanley, 1999). Both methods require great effort for sample preparation because imaging is carried out under vacuum conditions. High water content samples are therefore typically dried or frozen prior to measurement. The development of environmental SEM (E-SEM), however, has reduced the problems associated with artefact generation during sample preparation. These instruments are capable of obtaining images of specimens in a gaseous environment and, therefore allow the imaging of emulsions in their near natural state. Fig. 19 shows an example of an oil-in-water emulsion imaged by E-SEM (Stokes et al., 1998). The droplets of oil are seen as dark circles in the continuous phase of water.

In TEM, a cloud of electrons, produced by a tungsten cathode, is accelerated through a small aperture in a positively charged plate to form an electron beam. This beam is focused and directed through the specimen by a series of magnetic lenses. Part of the electron beam is either absorbed or scattered by the specimen, while the rest is transmitted. The beam of transmitted electrons is magnified by a magnetic lens and then projected onto a screen to create an image of the specimen. Electrons are highly attenuated by most materials and therefore one of the limitations of this technique is that the specimens must be extremely thin (approx. 0.05–0.1 µm) in order to allow enough of the electron beam to be detected.

SEM relies on the measurement of secondary electrons generated by a specimen when it is bombarded by an electron beam. In SEM, a focused electron beam is directed at a particular point on the surface of the specimen. Some energy associated with the electron beam is absorbed by the material and causes it to generate secondary electrons, which are recorded by a detector. An image is obtained by scanning the electron beam in an *x*–*y* direction over its surface and then recording the number of electrons generated at each location. Although sample preparation in SEM is difficult, it is considerably easier than for TEM and it has the advantage of producing fewer artefacts than the sample preparation for TEM since ultra thin samples are not required. However, the resolution of TEM can be between 0.2 and 1 nm, whilst SEM resolution is of the order of 3–6 nm.

TEM and SEM have been used widely to determine the size of emulsion droplets and the surface morphology of droplets (e.g. Mikula and Munoz, 2000; Li et al., 2009). Examples of the use of electron microscopy for the characterisation of emulsions generated in microchannels are, however, scarce. This mostly has to do with the difficulties related to sample preparation and the fact that on-line measurements are not possible. New techniques such as E-SEM, which has been applied successfully for the *in situ* monitoring of 'emulsion-like' structures (Rizzieri et al., 2003), may therefore be interesting for measuring drop characteristics in microchannels.

4.2.1.4. Atomic force microscopy (AFM). AFM can provide 3-dimensional imaging of surfaces with nanometer resolution. The AFM imaging principle is not optical and images are obtained by measuring changes in the magnitude of the interaction between the probe and the sample surface as the surface is scanned beneath the probe. A laser beam is focused onto the end of the cantilever, and then reflected onto a position-positive photodiode detector after being reflected by a mirror. When the sample is scanned, the topography of the sample surface causes the cantilever to deflect as the force between the tip and the sample changes. The map of the surface topography from the measured cantilever deflection is generated by computer and is shown on

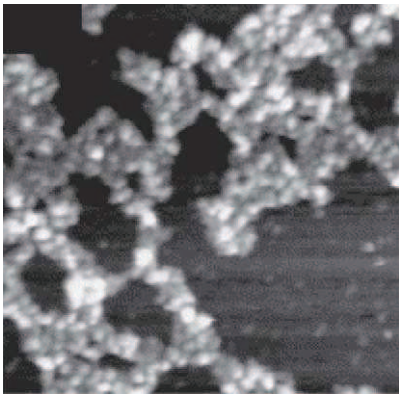

Fig. 20. Example of AFM for imaging the organisation of a surfactant at liquid–liquid interfaces. In this image a β-lactoglobulin film is displaced by surfactant Tween20 in an oil–water dispersion (Pugnaloni et al., 2004; reproduced with permission). The image is $0.8 \times 0.8\,\mu m$.

the monitor. In its usual mode of operation, the deflection of the cantilever is maintained at a predetermined value as the scan progresses in order to keep the forces acting between tip and sample constant. By monitoring the movements of the scanner that are required to maintain the deflection of the cantilever constant, the sample topography is revealed as a 3-dimensional image (Khulbe et al., 2008).

The lateral resolution of AFM depends mainly on tip sharpness, shape and size of the probe and image pixelization. The radius of curvature of the end of the tip will determine the highest lateral resolution obtainable with a specific tip; e.g., if the sample surface is an atomically flat periodic lattice, it would be possible to achieve atomic resolution. In commercial instruments, typical values of lateral resolution are on the order of nanometers, whilst the axial resolution is in the order of tenths of nanometers. A particular feature of AFM is the relatively small scan size (in the range of a few micrometers), which could be a limitation if the area of interest is relatively large. In addition, imaging requires long scanning time, which limits the application of AFM to low speed and static phenomena. Consequently AFM has not been applied to monitor droplet formation during emulsification.

Commercial instruments based on this technology are widely available and are increasingly being used in industry. The main applications of AFM to characterise emulsions are focused on measuring the local properties at the interface. With AFM or with AFM related set-ups, the electric double-layers at the droplet interface can be analysed, and it is possible to measure the force between an oil drop and the other immiscible liquid (Butt et al., 2005). AFM has also been used to visualise the molecular organization of emulsifiers at planar interfaces, as shown in Fig. 20, where imaging is employed to investigate the competitive adsorption of proteins and low-molecular-weight surfactants (Pugnaloni et al., 2004).

4.2.2. Static light scattering

Analytical instruments based on static light scattering have been commercially available for many years, and are widely used in industry for research, development, and quality control purposes. In particle size analysers that use static light scattering (also called laser diffraction), light from a laser is shone into a group of emulsion droplets; the droplets scatter the light, the smaller droplets scattering the light at larger angles than the bigger particles. The scattered light can be measured by a series of photodetectors placed at different angles. The angular dependency of the intensity of the light emerging from the emulsion is known as the diffraction pattern of the sample. By using a mathematical model to relate the diffraction pattern of the emulsion sample to the droplet characteristics, the particle size distribution and concentration are determined (Hiemenz and Rajagolapan, 1997). Although several correlations and theories exist on light scattering, the most comprehensive and rigorous theory is that of Mie, which is based on Maxwel's electromagnetic field equations that describe the propagation of an electromagnetic wave through an ensemble of particles. There are two assumptions made in this theory that are significant to the result obtained: (i) the particle is assumed to be spherical and (ii) the suspension is dilute. The particle concentration is assumed to be so low that scattered radiation is directly measured by the detector (i.e. single scattering) and not rescattered by other particles before reaching the detector (i.e. multiple scattering).

In modern particle sizing instruments, the scattering pattern recorded by the detectors is sent to a computer, where it is stored and analysed. The particle size distribution that gives the best fit between the experimental measurements and those predicted by Mie theory is calculated. This calculation requires information about the refractive index of both the droplets and the continuous phase at the wavelength of the laser used. The range of droplet size that can be measured using this kind of particle size analysers depends on the range of angles over which the instrument measures the intensity. Most commercial equipment is able to measure droplets with diameters in the range of 0.2–2000 μm (Hiemenz and Rajagolapan, 1997). As aforementioned, the fraction of the dispersed phase in the sample is required to be relatively low (< 0.1 wt%) to avoid multiple scattering effects. As a result, many emulsions need to be diluted significantly before analysis, which can cause appreciable alterations in particle size distribution, and this is particularly true for emulsions containing flocculated droplets.

In recent years, new mathematical algorithms have been developed to extend the concentration range over which laser diffraction can be used. Multiple light scattering has been reported to monitor droplet sizes in concentrated emulsions during ultrasound emulsification (Abismail et al., 2000). In addition, effective sample extraction and preparation systems have been designed to obtain a representative sample stream that is appropriate for analysis from a concentrated emulsion (Schmitt). In this way the applicability of the technique has been significantly extended and commercial equipment with flow through cells for measurements in industrial emulsification devices are available. For example, the direct measurement of the drop size distributions and concentration of the oil-in-water emulsions that make up oil rig effluent streams may be undertaken in-line using a high-pressure cell (10 bar maximum operating pressure). The recent developments of this technique and the possibility to carry out in-line measurements pave a promising future for its application to continuous microchannel equipment.

4.2.3. Dynamic light scattering (DLS) and diffusing wave spectroscopy (DFW)

When a beam of light passes through an emulsion, the droplets scatter some of the light in all directions. When the particles are very small compared with the wavelength of the light, the intensity of the scattered light is uniform in all directions (Rayleigh scattering). If the light is coherent and monochromatic, as it is from a laser, it is possible to observe time-dependent fluctuations in the scattered intensity using a suitable detector, such as a photomultiplier that is capable of operating in photon counting mode. These fluctuations arise from the fact that the particles are small enough to undergo random thermal (Brownian) motion and the distance between them is therefore

constantly varying. Constructive and destructive interference of light scattered by neighbouring particles within the illuminated zone gives rise to the intensity fluctuation at the detector plane which contains information about droplet motion. Analysis of the time dependency of the intensity fluctuation can therefore yield the diffusion coefficient of the droplets from which, via the Stokes Einstein equation and with knowledge of the viscosity of the medium, the hydrodynamic radius or diameter of the droplets can be calculated (Horne, 1995). The diameter obtained by this technique is that of a sphere that has the same translational diffusion coefficient as the particle being measured. The translational diffusion coefficient will depend not only on the size of the particle 'core', but also on any surface structure, as well as the concentration and the type of ions in the medium. This means that the size can be larger than that measured by electron microscopy, for example, where the particle is removed from its native environment.

Commercial analytical instruments based on dynamic light scattering instruments (photon correlation spectroscopy and Doppler shift spectroscopy) have mostly been developed to analyse emulsions where the laser beam undergoes single scattering before reaching the detector. These droplet size analysers can determine droplet diameters between 3 nm and 5 μm. The maximum concentration of dispersed phase that the sample can have depends however on the method used by the DLS equipment to measure the scattered light intensity fluctuations (Horne, 1995). Some instruments measure the light that has been transmitted through an emulsion and are therefore only suitable for analysis of dilute emulsions (<0.1 wt% of dispersed phase). Other instruments measure the light that has been backscattered from an emulsion and are therefore suitable for analysis of dilute and concentrated emulsions (up to 10 wt% of dispersed phase).

A more recent technique, diffusing wave spectroscopy (DWS) must operate in a highly turbid medium (or "multiple scattering" regime) because it treats the photon path through the sample as a diffusive process. In other words, with this extensive multiple scattering, the light waves move through the system in a way that can be modelled mathematically as a diffusion process (Scheffold, 2002). Similar to dynamic light scattering, DWS is able to provide information about the local dynamics of droplet emulsions, without restrictions on droplet concentration and turbidity. DWS has been used to provide information about physicochemical phenomena that influence the mobility of emulsion droplets, for instance, droplet size, droplet–droplet interactions (Hemar and Horne, 1999), flocculation (Hemar et al., 2003), interface properties (Wooster and Augustin, 2006) or changes in continuous phase rheology (Harden and Viasnoff, 2001). This technique is also capable of following the kinetics of destabilization of concentrated emulsions. In addition, it can detect differences at the microstructural level between the different types of destabilization processes, without any sample disturbance and at concentrations close to the reality of formulations used in industrial processes.

4.2.4. Electric pulse counting

Electrical pulse counting techniques (also called electrozone sensing or Coulter counter techniques) are based on measurable changes in electrical resistance produced by droplets, with much lower electrical conductivity than the continuous phase, suspended in an electrolyte. In the sensing zone each particle displaces its own volume of electrolyte. The volume displaced is measured as a voltage pulse; the height of each pulse is proportional to the volume of the particle. These techniques are capable of determining the size distribution of droplets between 0.4 and 1200 μm (Mikula, 1992).

In order to size an emulsion, a sample of it must be probed with two electrodes. One electrode is placed within a glass tube that has a small hole in it, though which the emulsion is sucked. The electrical pulse created by each droplet, due to the lower electrical conductivity than the continuous phase, is recorded and its size is calculated. Typically, droplets between 2 and 60% of the diameter of the aperture can be reliably analysed. If an emulsion contains a wide range of droplet sizes it may be necessary to use a number of glass tubes with different aperture sizes to determine the full droplet size distribution. Equipment based on this principle has been commercially available for many years and is widely used in industry.

This technique presents some limitations that have to be considered depending on the characteristics of the emulsion to be analysed (Lines, 1994). Electrical pulse counting instruments normally require the droplet concentration to be relatively low (<0.1 wt%) so that only a single particle passes through the hole at time. Consequently, emulsions with a higher concentration need to be diluted before analysis, which may alter the sample microstructure. In addition, the emulsion droplets must be suspended in an electrolyte solution to ensure that the electrical conductivity of the aqueous phase is sufficiently large to obtain accurate measurements.

4.2.5. Ultrasonic spectroscopy

The interactions between ultrasonic waves and emulsions are used to obtain information about droplet size distributions and concentration. Ultrasonic spectroscopy relies on measurements of the change in ultrasonic attenuation and/or ultrasonic velocity as a function of frequency. As an ultrasonic wave propagates through an emulsion some of the ultrasonic wave energy is lost; the characteristics of this will depend on the thermophysical properties of the component phases, the frequency of the ultrasonic wave, and the concentration and size of the droplet.

The operating principles of an ultrasonic spectrometer are straightforward. The equipment generates sound pulses that pass through a sample system and then measured by a receiver. The passage through the sample system causes the sound energy to change in intensity and phase. The instrument measures the ultrasonic attenuation (sound energy losses) and the ultrasonic velocity (sound speed). The analysis of the attenuation data to obtain droplet size distributions involve a degree of complexity in fitting experimental results to theoretical models based on various acoustic loss mechanisms. Ultrasonic spectroscopy instruments contain the mathematical models that can predict the ultrasonic spectrum of an emulsion from the droplet characteristics (size, concentration) and the physical properties of the dispersed and continuous phases, such as ultrasonic velocity, ultrasonic attenuation, thermal conductivity, specific heat capacity, thermal expansion coefficient, density and viscosity (Dukhin and Goetz, 2006).

Commercial ultrasonic spectrometers size emulsion droplets with diameters between 10 nm and 1000 μm and are able to provide reliable droplet size information of both concentrated (above 40% phase volume fraction) and diluted (phase volume fractions of 0.1%) emulsions. Ultrasound is a non-destructive and non-intrusive technique that has been successfully applied to determine the droplet size distributions and concentrations in food emulsions (e.g., (Coupland and McClements, 2004) and microemulsions (Dukhin and Goetz, 2001)). A major advantage of ultrasonic spectroscopy is that it is transparent to most materials and can be used to analyse emulsions *in situ*; it is therefore

particularly suitable for on-line measurements (e.g., (Gancz et al., 2006)).

The main limitations of the ultrasonic technique are related to the high amount of thermophysical data required to interpret the results and the fact that small air bubbles can interfere with the signal from the emulsion droplets (Coupland and McClements, 2004).

4.2.6. Nuclear magnetic resonance (NMR)

In emulsion characterization, NMR is used to measure self-diffusion, which is exploited to determine droplet size distribution. The measurement of self-diffusion of molecules in a liquid by NMR relies on the use of magnetic field gradients. NMR techniques use interactions between radio waves and the nuclei of, typically, hydrogen atoms. The sample to be analysed is placed in a static magnetic field gradient and a sequence of radio frequency pulses is applied to it. These pulses cause some of the hydrogen nuclei in the sample to be excited to higher energy levels, which generates a detectable NMR signal. The decay of this signal depends on the movement of the nuclei sample and can be used to study molecular motion.

In a bulk liquid, the distance that a molecule can move in a certain time is governed by its translational diffusion coefficient. When a liquid is contained in an emulsion droplet, its diffusion may be restricted by the interfacial droplet boundary. If the movement of a molecule in the droplet is observed over a long time, the diffusion is restricted because the molecule cannot move further than the droplet diameter. Considering this, it is possible to identify when the diffusion becomes restricted by measuring the attenuation of the NMR signal at different times. From this time-resolved signal, the emulsion droplet size distribution and structural organization of the droplets within an emulsion can be inferred (Johns and Hollingsworth, 2007).

NMR measurements are not influenced by the optical or dielectric properties of the system. Therefore, both transparent and opaque emulsions and dispersions can be tested in optically opaque devices. Low-frequency NMR spectrometers operating at 2–20 MHz suffice for time-resolved signal applications and are most commonly used in industrial applications. The range of droplet sizes that can be determined precisely with these methods is between 0.2 and 100 μm and a typical NMR test can take between 1 and 20 min. The advantages of this technique are that it is non-intrusive and requires only a small sample size (0.5 g approx.) without any further preparation (Peña and Hirasaki, 2006).

NMR methods are particularly adapted for sizing opaque and very viscous emulsions such as water-in-crude oil emulsions and food emulsions (Johns and Hollingsworth, 2007), which are not readily suitable to alternative droplet sizing techniques. In addition, the NMR technique is particularly useful to determine the actual size of the individual droplets in flocculated emulsions (Lee et al., 1998). It has also been applied to monitor droplet growth in emulsions due to droplet coalescence and Ostwald ripening (e.g., Hedin and Furo, 2001; Peña et al., 2005). Additionally, there has been some development of the NMR technique for the characterisation of emulsions in dynamic flow conditions and for *in situ* measurements. Johns and Gladden (2002) developed a flow-compensating pulsed field gradient that enables the drop size distribution of emulsions in continuous laminar flow to be characterised. Hollingsworth et al. (2004) reported a NMR method that enables fast measurement of drop size, thus allowing the time evolution of drop size distribution to be determined *in situ*. Although the characterisation of liquid–liquid dispersions in microchannels using NMR methods has not yet been reported, the recent developments of this technique with respect to fast *in situ* measurements and continuous flow systems suggest that it is a promising method for future microchannel applications.

4.2.7. Electroacoustics

Electroacoustic spectroscopy deals with the interaction of electric and acoustic fields. When the charged particles of a dispersed system are placed in an acoustic field, they lead to the generation of an alternating electric field, and consequently to an alternating electric current. Considering this, two possible implementations of electroacoustic spectroscopy can be distinguished. One can apply an acoustic field and measure the resultant electric current, which is referred to as the colloid vibration current (CVC), or one can apply an electric field and measure the resultant acoustic field, which is referred to as the electronic sonic amplitude (ESA).

Both electroacoustic parameters, CVC and ESA, can be experimentally measured. The CVC or ESA spectrum is the experimental output from electroacoustic spectroscopy. Both of these spectra contain information about droplet size distribution and zeta potential, which is related to the electrical charge of the droplet. Particle/drop sizing instruments based on the electroacoustic principle are commercially available and are capable of analysing droplets with sizes between 0.1 and 10 μm. By combining electroacoustic spectroscopy with ultrasonic spectroscopy the droplet size range can be extended from 10 nm to 1000 μm (Dukhin et al., 2000).

The major advantage of electroacoustic techniques is that they can be applied to concentrated emulsions (up to 50% phase volume fraction) without the need of any sample dilution. Nevertheless, they can only be used to analyse emulsion droplets that are charged and that have a significant density difference to the surrounding liquid and, the viscosity of the continuous phase must be known at the measurement frequency.

Electroacoustics have been applied to measure particle size distributions and, in some cases the zeta potential of emulsion droplets, in a wide variety of different oil-in-water (e.g., Hunter, 2001, Hsu and Nacu, 2003) and water-in-oil emulsions (e.g., Magual et al., 2005). Some commercial instruments have been developed for on-line processes.

5. Conclusions

This review reports the existing experimental methods available for characterising mixing, and the outcomes of mixing, of miscible and immiscible liquids, as well as gas–liquid flows in micro devices. Some of the these techniques have been adopted from the characterisation methods commonly used in chemical engineering for assessing macroscopic flow systems (see for example Fournier et al., 1996; Thakur et al., 2003; Boyer et al., 2002; Chaouki et al., 1997); others are modifications of methods originally developed in the field of biology (e.g., techniques based microscopy) or analytical chemistry (e.g., UV–Vis and IR spectroscopy, NMR). The report provides concise information on each method concerning the main principles, the type of information obtained, the limitations of the technique, and some referenced examples. In this format, it is hoped that the review will help guide the micro device user (industrial or academic) in the choice of mixing characterisation methods that are appropriate for the device and the application (single or multiphase), and that enable the required information to be obtained. In addition, this review highlights the limitations of these existing methodologies, thus allowing the mixing performance characteristics that are not yet measurable with the existing techniques to be identified.

The limitations of the existing characterisation techniques are particularly important to understand for industrial applications of

micro devices. From this review, it can be seen that the majority of the experimental techniques available for characterising mixing and two-phase flows employ optical methods, which require that the micro device is transparent or has a transparent viewing window. In the process industries, however, transparent construction materials may not be entirely adapted for the harsh environment of the chemical and physical processes encountered and these characterisation methods may not be applicable. This shows the importance of coupling academic-type studies with industrial problems, when possible, for the improvement and control of process performance. Needless to say, the monitoring of industrial mixing and contacting operations may still of course be required for the adequate control of process performance. For single phase mixing operations the direct characterisation of mixing performance most likely will not be feasible, although concentration measurements that provide indirect information on the mixing quality may be more easily accessible using conventional analytical techniques or integrated non-intrusive sensors. For the monitoring of gas–liquid flow in industrial micro devices non-intrusive sensors that do not require direct optical access to the flow are required. Some development in this area has been started, as previously mentioned in the body of this review. Additionally, it is worth mentioning the possibility of employing methods that are already successfully applied for the characterisation of macro scale operations. In particular electrodiffusion diagnostics is a useful non-intrusive, non-optical tool for monitoring near-wall flow and gas–liquid flow regimes, as well as for the measurement of the bubble size and bubble velocity in macro scale devices (Kashinsky and Randin, 1999; Magaud et al., 2001; Michele and Hempel, 2002). Its application to the measurement of single flow in microchannels has already been demonstrated and extending its application to gas–liquid flows in micro devices is expected to be relatively straight forward. For characterising liquid–liquid dispersions and emulsions, most available methods require either optical access to the sample and sample dilution, thus off-line characterisation. Currently, the most widely used techniques for drop characterisation are microscopy-based methods that do not require difficult sample preparation. These are important experimental techniques since they allow information concerning emulsion structure, as well as dynamic processes such as drop formation and coalescence mechanisms to be obtained *in situ*. In particular, CSLM is of great interest since it can provide 3-dimensional information on the emulsion structure. Ultrasonic spectroscopy and NMR may be promising methods for the on-line monitoring of liquid–liquid dispersions in micro devices as they allow *in-situ* measurements without requiring optical access to the liquid–liquid dispersion. Static light scattering methods that can be used on-line with flow through cells may also be useful. Further developments of these methods may be needed for their application to the characteristic size of micro devices.

Acknowledgements

This work was funded by the Integrated Project IMPULSE (Project no. NMP2-CT-2005-011816), www.impulse-project.net, within the 6th Framework Programme of the European Commission.

References

Abismail, B., Canselier, J.P., Wilhelm, A.M., Delmas, H., Gourdon, C., 2000. Emulsification processes: on-line study by multiple light scattering measurements. Ultrason. Sonochem. 7 (4), 187–192.

Aguilera, J.M., Stanley, D.W., 1999. Microstructural Principles of Food Processing and Engineering. Aspen Publishers, Maryland.

Ahola, S., Casanova, F., Perlo, J., Münnemann, K., Blümich, B., Stapf, S., 2006. Monitoring of fluid motion in a micromixer by dynamic NMR microscopy. Lab Chip 6, 90–95.

Aoki, N., Mae, K., 2006. Effects of channel geometry on mixing performance of micromixers using collision of fluid segments. Chem. Eng. J. 118, 189–197.

Bottausci, F., Cardonne, C., Meinhart, C., Mezic, I., 2007. An ultrashort mixing length micromixer: the shear superposition micromixer. Lab Chip 7, 396–398.

Bourne, J.R., Kut, O.M., Lenzner, J., 1992. An improved reaction system to investigate micromixing in high-intensity mixers. Ind. Eng. Chem. Res. 31, 949–958.

Baldyga, J., Bourne, J.R., 1999. Turbulent Mixing and Chemical Reactions. Wiley, New York.

Bown, M.R., MacInnes, J.M., Allen, R.W.K., Zimmerman, W.B.J., 2006. Three-dimensional, three-component velocity measurements using stereoscopic micro-PIV and PTV. Meas. Sci. Tech. 17, 2175–2185.

Boyer, C., Duquenne, A.-M., Wild, G., 2002. Measuring techniques in gas–liquid and gas–liquid–solid reactors. Chem. Eng. Sci. 57, 3185–3215.

Branebjerg, J., Fabius, B., Gravesen, B., 1995. Application of miniature analysers: from microfluidic components to μTAS. In: Van den Berg, A., Bergfeld, P. (Eds.), Micro Total Analysis Systems. Kluwer, Dordrecht, pp. 141–151.

Brujic, J., Edwards, S.F., Grinev, D.V., Hopkinson, I., Brujic, D., Makse, H.A., 2003a. 3D bulk measurements of the force distribution in a compressed emulsion system. Faraday Discuss. 123, 207–220.

Brujic, J., Edwards, S.F., Hopkinson, I., Makse, H.A., 2003b. Measuring the distribution of interdroplet forces in a compressed emulsion system. Phys. A Stat. Mech. Appl. 327 (3–4), 201–212.

Butt, H.J., Cappella, B., Kappl, M., 2005. Force measurements with the atomic force microscope: technique, interpretation and applications. Surf. Sci. Rep. 59 (1–6), 1–152.

Cha, J., Kim, J., Ryu, S.-K., Park, J., Jeong, Y., Park, Se., Park, Su., Kim, H.C., Chun, K., 2006. A highly efficient 3D micromixer using soft PDMS bonding. J. Micromech. Microeng. 16, 1778–1782.

Chaouki, J., Larachi, F., Dudukovic, M.P., 1997. Non invasive tomographic and velocimetric monitoring of multiphase flows. Ind. Eng. Chem. Res. 36, 4476–4503.

Coupland, J.N., McClements, D.J., 2004. Analysis of droplet characterstics using low-intensity ultrasound. In: Fribergs, Larsson, K., Sjoblon, J. (Eds.), Food Emulsions fourth ed. Marcel Dekker, New York.

Cristobal, G., Arbouet, L., Sarrazin, F., Talaga, D., Bruneel, J.-L., Joanicot, M., Servant, L., 2006. On-line laser Raman spectroscopic probing of droplets engineered in microfluidic devices. Lab Chip 6, 1140–1146.

Cubaud, T., Ulmanella, U., Ho, C.-M., 2006. Two-phase flow in microchannels with surface modifications. Fluid Dyn. Res. 38, 772–786.

Danckwerts, P.V., 1952. The definition and measurement of some characteristics of mixtures. Appl. Sci. Res. A 3, 279–296.

de Mas, N., Günther, A., Kraus, T., Schmidt, M.A., Jensen, K.F., 2005. Scaled-out multilayer gas–liquid microreactor with integrated velocimetry sensors. Ind. Eng. Chem. Res. 44, 8997–9013.

Devasenathipathy, S., Santiago, J.G., Wereley, S.T., Meinhart, C.D., Takehara, K., 2003. Particle imaging techniques for microfabricated fluidic systems. Exp. Fluids, 34, 504–514.

Dickinson, E., Radford, S.J., Golding, M., 2003. Stability and rheology of emulsions containing sodium caseinate: combines effects of ionic calcium and non-ionic surfactant. Food Hydrocolloids 17, 211–220.

Dukhin, A.S., Goetz, J.P., 2001. Acoustic and electroacoustic spectroscopy for characterizing concentrated dispersions and emulsions. Adv. Colloid Interface Sci. 92, 73–132.

Dukhin, A.S., Goetz, J.P., 2006. Ultrasound for characterizing emulsions and microemulsions. In: Sjoblon, J. (Ed.), Emulsions and Emulsion Stability second ed CRC Press, Boca-Raton, pp. 311–353.

Dukhin, A.S., Goetz, P.J., Wines, T.H., Somasundaran, P., 2000. Acoustic and electroacoustic spectroscopy. Colloids and Surf. A Physicochemical Eng. Aspects 173 (1–3), 127–158.

Ehlers, S., Elgeti, K., Menzel, T., Weissmeier, G., 2000. Mixing in the offstream of a microchannel system. Chem. Eng. Proc. 39, 291–298.

Ehrfeld, W., Golbig, K., Hessel, V., Löwe, H., Richter, T., 1999. Characterisation of mixing in micromixers by a test reaction: single mixing units and mixer arrays. Ind. Eng. Chem. Res. 38, 1075–1082.

Ehrfeld, W., Hessel, V., Löwe, H., 2000. Microreactors: New Technology for Modern Chemistry. Wiley, Weinheim.

Falk, L., Commenge, J.-M., 2010. Performance comparison of micromixers. Chem. Eng. Sci. 65, 405–411.

Ferrando, M., Spiess, W.E.L., 2000. Review: confocal scanning laser microscopy. A powerful tool in food science. Food Sci. Technol. Int. 6 (4), 267–284.

Fletcher, D.F., Haynes, B., Aubin, J., Xuereb, C., 2009. Modelling of micro-fluidic devices. In: Hessel, V., Schoten, J.C., Renken, A., Yoshida, J.-I. (Eds.), Handbook of Micro Reactors, Vol. A: Fundamentals, Operations & Catalysts. Wiley, Weinheim, pp. 117–144 (Chapter 5).

Fournier, M.C., Falk, L., Villermaux, J., 1996. A new parallel competing reaction system for assessing micromixing efficiency—experimental approach. Chem. Eng. Sci. 51, 5053–5064.

Fries, D.M., Waellchli, S., von Rohr, P.R., 2008. Gas–liquid two-phase flow in meandering microchannels. Chem. Eng. J. 135S, S37–S45.

Gancz, K., Alexander, M., Corredig, M., 2006. In situ study of flocculation of whey protein-stabilized emulsions caused by addition of high methoxyl pectin. Food Hydrocolloids 20 (2–3), 293–298.
Gladden, L.F., Mantle, M.D., Sederman, A.J., 2005. Quantifying physics and chemistry at multiple length-scales using magnetic resonance techniques. In: Marin, G.B. (Ed.), Advances in Chemical Engineering: Multiscale Analysis, vol. 30. Elsevier, pp. 63–135.
Guichardon, P., Falk, L., 2000. Characterisation of micromixing efficiency by the iodide-iodate reaction system. Part I. Experimental procedure. Chem. Eng. Sci. 55, 4233–4243.
Guillot, P., Colin, A., 2005. Stability of parallel flows in a microchannel after a T-junction. Phys. Rev. E 72 066301(1-4).
Günther, A., Khan, S.A., Thalmann, M., Traschsel, F., Jensen, K.F., 2004. Transport and reaction in microscale segmented gas–liquid flow. Lab Chip 4, 278–286.
Hanratty, T.J., Campbell, J.A., 1983. Measurement of wall shear stress. In: Goldstein, J.R. (Ed.), Fluid Mechanics Measurement, Hemisphere. Washington, pp. 559–615.
Harden, J.L., Viasnoff, V., 2001. Recent advances in DWS-based micro-rheology. Curr. Opinion Colloid Interface Sci. 5–6, 438–445.
Hardt, S., Pennemann, H., Schönfeld, F., 2006. Theoretical and experimental characterization of a low-Reynolds number split-and-recombine mixer. Microfluid Nanofluid 2, 237–248.
Haverkamp, V., Hessel, V., Löwe, H., Menges, G., Warnier, M.J.F., Rebrov, E.V., de Croon, M.H.J.M., Schouten, J.C., Liauw, M.A., 2006. Hydrodynamics and mixer-induced bubble formation in micro bubble columns with single and multi-phase channels. Chem. Eng. Technol. 29, 1015–1026.
Hedin, N., Furo, I., 2001. Ostwald ripening of an emulsion monitored by PGSE NMR. Langmuir 17, 4746.
Heertje, I., van Aalst, H., Blonk, J.C.G., Don, A., Nederlof, J., Lucassen-Reynders, E.H., 1996. Observations on emulsifiers at the interface between oil and water by confocal scanning light microscopy. Lebensm.-Wiss. u.-Technol. 29, 217–226.
Hemar, Y., Horne, D.S., 1999. A diffusing wave spectroscopy study of the kinetics of Ostwald ripening in protein-stabilized oil/water emulsions. Colloids Surf. B 12, 239–246.
Hemar, Y., Pinder, D.N., Hunter, R.J., Singh, H., Hebraud, P., Horne, D.S.J., 2003. Monitoring of flocculation and creaming of sodium-caseinate-stabilized emulsions using diffusing-wave spectroscopy. Colloid Interface Sci. 264, 502–508.
Hessel, V., Hardt, S., Löwe, H., Schönfeld, F., 2003. Laminar mixing in different interdigital micromixers: I. Experimental characterization. A.I.Ch.E. J. 49 (3), 566–577.
Hessel, V., Löwe, H., Schönfeld, F., 2005. Micromixers—a review on passive and active mixing principles. Chem. Eng. Sci. 60, 2479–2501.
Hiemenz, P.C., Rajagolapan, R., 1997. Principles of Colloid and Surface Chemistry, third ed. Marcel Dekker, New York, NY.
Hoffmann, M., Schülter, M., Räbiger, N., 2006. Experimental investigation of liquid–liquid mixing in T-shaped micro-mixers using μ-LIF and μ-PIV. Chem. Eng. Sci. 61, 2968–2976.
Hollingsworth, K.G., Sederman, A.J., Buckley, C., Gladden, L.F., Johns, M.L., 2004. Fast emulsion droplet sizing using NMR self-diffusion measurements. J. Colloid Interface Sci. 274, 244–250.
Horne, D.S., 1995. Light scattering studies of colloid stability and gelation. In: Dickinson, E. (Ed.), New Physicochemical Techniques for the Characterization of Complex Food Systems. Blackie Academic and Professional, London, UK.
Hsu, J.P., Nacu, A., 2003. Behavior of soybean oil-in-water emulsion stabilized by nonionic surfactant. J. Colloid Interface Sci. 259, 374–381.
Huchet, F., Comiti, J., Tihon, J., Montillet, A., Legentilhomme, P., 2007. Electro-diffusion diagnostics of the flow and mass transfer inside a network of crossing minichannels. J. Appl. Electrochem. 37, 49–55.
Hunter, R.J., 2001. Measuring zeta potential in concentrated industrial slurries. Colloids Surf. A Physicochem. Eng. Aspects 195 (1–3), 205–214.
Johns, M.L., Gladden, L.F., 2002. Sizing of emulsion droplets under flow using flow-compensated NMR-PFG techniques. J. Magn. Reson. 154 (1), 142–145.
Johns, M.L., Hollingsworth, K.G., 2007. Characterisation of emulsion systems using NMR and MRI. Prog. Nucl. Magn. Reson. Spectros. 50, 51–70.
Johnson, T.J., Ross, D., Locascio, L.E., 2002. Rapid microfluidic mixing. Anal. Chem. 74 (1), 45–51.
Kashinsky, O.N., Randin, V.V., 1999. Downward bubbly gas–liquid flow in a vertical pipe. Int. J. Multiphase Flow 25, 109–138.
Keoschkerjan, R., Richter, M., Boskovic, D., Schnürer, F., Löbbecke, S., 2004. Novel multifunctional microreaction unit for chemical engineering, Chem. Eng. J. 101, pp. 469–475.
Khulbe, K.C., Feng, C.Y., Matsuura, T., 2008. Synthetic Polymeric Membranes: Characterization by Atomic Force Microscopy. Springer, Berlin, Heidelberg.
Kim, D.S., Lee, S.W., Kwon, T.H., Lee, S.S., 2004. A barrier embedded Kenics micromixer. J. Micromech. Microeng. 14, 1294–1301.
King, C., Walsh, E., Grimes, R., 2007. PIV measurements of flow within plugs in a microchannel. Microfluid Nanofluid 3, 463–472.
Kinoshita, H., Kaneda, S., Fujii, T., Oshima, M., 2007. Three-dimensional measurement and visualisation of internalflow of a moving droplet using confocal micro-PIV. Lab Chip 7, 338–346.
Knight, J.B., Vishwanath, A., Brody, J.P., Austin, R.H., 1998. Hydrodyanmic focusing on a silicon chip: mixing nanoliters in microseconds. Phys. Rev. Lett. 80 (17), 3863–3866.
Kockmann, N., Kiefer, T., Engler, M., Woias, P., 2006. Silicon microstructures for high throughput mixing devices. Microfluid Nanofluid 2, 327–335.
Koo, H.Y., Chang, S.T., Choi, W.S., 2006. Emulsion-based synthesis of reversibly swellable, magnetic nanoparticle-embedded polymer microcapsules. Chem. Mater. 18 (14), 3308–3313.
Kraus, T., Günther, A., de Mas, N., Schmidt, M.A., Jensen, K.F., 2004. An integrated multiphase flow sensor for microchannels. Exp. Fluids 36, 819–832.
Kristal, J., 2008. Study of gas–liquid flow in the thin-gap channel. Ph.D. Dissertation, Institute of Chemical Technology, Prague, Czech Republic.
Kristal, J., Kodym, R., Bouzek, K., Jiricny, V., 2008. Electrochemical microreactor and gas-evolving reactions. Electrochem. Commun. 10, 204–207.
Kukukova, A., Aubin, J., Kresta, S.M., 2009. A new definition of mixing and segregation: three dimensions of a key process variable. Chem. Eng. Res. Des. 87 (A4), 633–647.
Lee, H.Y., McCarthy, M.J., Dungan, S.R., 1998. Experimental characterization of emulsion formation and coalescence by nuclear magnetic resonance restricted diffusion techniques. J. Am. Oil Chem. Soc. 75, 463–475.
Lee, S.W., Kim, D.S., Lee, S.S., Kwon, T.H., 2006. A split and recombination micromixer fabricated in a PDMS three-dimensional structure. J. Micromech. Microeng. 16, 1067–1072.
Leung, S.-A., Edel, J.B., Wootton, R.C.R., de Mello, A.J., 2004. Continuous real-time bubble monitoring in microchannels using refractive index detection. Meas. Sci. Technol. 15, 290–296.
Li, X.W., Zhang, J., Zheng, L.Q., Chen, B., Wu, L.Z., Lv, F.F., Dong, B., Tung, C.H., 2009. Microemulsions of N-alkylimidazolium ionic liquid and their performance as microreactors for the photocycloaddition of 9-substituted anthracenes. Langmuir 25, 5484–5490.
Lindken, R., Westerweel, J., Wieneke, B., 2006. Stereoscopic micro particle image velocimetry. Exp. Fluids 41, 161–171.
Lines, R.W., 1994. The electrical sensing zone method (the Coulter principle). In: Knapp, J.Z. (Ed.), Liquid and Surface Bourne Particle Measurement Handbook. Marcel Dekker, New York.
Liu, D., Garimella, S.V., Wereley, S.T., 2005. Infrared micro-particle image velocimetry in silicon-base microdevices. Exp. Fluids 38, 385–392.
Liu, R.H., Stremler, M.A., Sharp, K.V., Olsen, M.G., Santiago, J.G., Adrian, R.J., 2000. Passive mixing in a three-dimensional serpentine microchannel. J. Microelectromech. Sys. 9 (2), 190–197.
Magaud, F., Souhar, M., Wild, G., Boisson, N., 2001. Experimental study of bubble column hydrodynamics. Chem. Eng. Sci. 56, 4597–4607.
Magual, A., Horvath-Szabo, G., Masliyah, J.H., 2005. Acoustic and electroacoustic spectroscopy of water-in-diluted-bitumen emulsions. Langmuir 21 (19), 8649–8657.
Masca, S.I., Rodriguez-Mendieta, I.R., Friel, C.T., Radford, S.E., Smith, D.A., 2006. Detailed evaluation of the performance of microfluidic T mixers using fluorescence and ultraviolet resonance Raman spectroscopy. Rev. Sci. Instrum. 77, 055105.
Maynes, D., Webb, A.R., 2002. Velocity profile characterization in sub-millimeter diameter tubes using molecular tagging velocimetry. Exp. Fluids 32, 3–15.
Meinhart, C.D., Wereley, S.T., Santiago, J.G., 1999. PIV measurements of a microchannel flow. Exp. Fluids 27, 414–419.
Mensinger, H., Richter, T., Hessel, V., Döpper, J., Ehrfeld, W., 1995. Microreactor with integrated static mixer and analysis system. In: Van den Berg, A., Bergfeld, P. (Eds.), Micro Total Analysis Systems. Kluwer, Dordrecht, pp. 237–243.
Michele, V., Hempel, D.C., 2002. Liquid flow and phase holdup—measurement and CFD modeling for two-and three-phase bubble columns. Chem. Eng. Sci. 57, 1899–1908.
Mikula, R.J., 1992. Emulsion characterization. In: Schramm, L.L. (Ed.), Emulsions: Fundamentals and Applications in the Petroleum Industry. American Chemical Society, Washington, DC.
Mikula, R.J., Munoz, V.A., 2000. Characterization of emulsions and suspensions in the petroleum industry using cryo-SEM and CLSM. Colloids Surf. A Physicochem. Eng. Aspects 174, 23–36.
Mizushina, T., 1971. The electrochemical method in transport phenomena. In: Irvine, T.F., Harnett, J.P. (Eds.), Advances in Heat Transfer. Academic Press, New York, pp. 87–161.
Mosier, B.P., Molho, J.L., Santiago, J.G., 2002. Photobleached-fluorescence imaging of microflows. Exp. Fluids 33, 545–554.
Murphy, D.B., 2001. Fundamentals of Light Microscopy and Electronic Imaging, first ed. Wiley-Liss, New York.
Nagasawa, H., Aoki, N., Mae, K., 2005. Design of a new micromixer for instant mixing based on the collision of micro segments. Chem. Eng. Technol. 28, 324–330.
Panic, S., Loebbecke, S., Tuercke, T., Antes, J., Boskovic, D., 2004. Experimental approaches to a better understanding of mixing performance of microfluidic devices. Chem. Eng. J. 101, 409–419.
Park, J.S., Kihm, K.D., 2006. Three-dimensional micro-PTV using deconvolution microscopy. Exp. Fluids 40, 491–499.
Paul, E.L., Atiemo-Obeng, V., Kresta, S.M. (Eds.), 2004. Handbook of Industrial Mixing. Wiley, Hoboken, NJ.
Peña, A., Hirasaki, G.J., 2006. NMR characterization of emulsions. In: Sjöblom, J. (Ed.), Emulsions and Emulsion Stability. CRC Press, Boca-Raton, pp. 283–309.
Peña, A., Hirasaki, G.J., Miller, C.A., 2005. Chemically induced destabilization of water-in-crude oil emulsions. Ind. Eng. Chem. Res. 44 (5), 1139.
Pugnaloni, L.A., Dickinson, E., Ettelaie, R., 2004. Competitive adsorption of proteins and low-molecular-weight surfactants: computer simulation and microscopic imaging. Adv. Colloid Interface Sci. 107 (1), 27–49.

Raguin, L.G., Ciobanu, L., 2007. Multiple echo NMR velocimetry: fast and localized measurements of steady and pulsatile flows in small channels. J. Magn. Reson. 184, 337–343.
Revellin, R., Agostini, B., Ursenbacher, T., Thome, J.R., 2008. Experimental investigation of velocity and length of elongated bubbles for flow of R-134a in a 0.5 mm microchannel. Exp. Thermal Fluid Sci. 32, 870–881.
Revellin, R., Dupont, V., Ursenbacher, T., Thome, J.R., Zun, I., 2006. Characterization of diabatic two-phase flows in microchannels: flow parameter results for R-134a in a 0.5 mm channel. Int. J. Multiphase Flow 32, 755–774.
Rizzieri, R., Baker, F.S., Donald, A.M., 2003. A study of the large strain deformation and failure behaviour of mixed biopolymer gels via in situ ESEM. Polymer 44, 5927–5935.
Roetmann, K., Schmunk, W., Garbe, C.S., Beushausen, V., 2008. Micro-flow analysis by molecular tagging velocimetry and planar Raman-scattering. Exp. Fluids 44, 419–430.
Romero, A., Cordobes, F., Puppo, M.C., Guerrero, A., Bengoechea, C., 2008. Rheology and droplet size of emulsions stabilized by crayfish flour. Food Hydrocolloids 22, 1033–1043.
Salman, W., Gavriilidis, A., Angeli, P., 2006. On the formation of Taylor bubbles in small tubes. Chem. Eng. Sci. 61, 6653–6666.
Salmon, J.-B., Ajdari, A., Tabeling, P., Servant, L., Talaga, D., Joanicot, M., 2005. In situ Raman imaging of interdiffusion in a microchannel. App. Phys. Lett. 86, 094106.
Santiago, J.G., Wereley, S.T., Meinhart, C.D., Beebe, D.J., Adrian, R.J., 1998. A particle image velocimetry system for microfluidics. Exp. Fluids 25, 316–319.
Sarrazin, F., Loubière, K., Prat, L., Gourdon, C., Bonometti, T., Magnaudet, J., 2006. Experimental and numerical study of droplets hydrodynamics in microchannels. A.I.Ch.E. J. 52, 4061–4070.
Sarrazin, F., Prat, L., Di Miceli, N., Cristobal, G., Link, D.R., Weitz, D.A., 2007. Mixing characterization inside microdroplets engineering on a microcoalescer. Chem. Eng. Sci. 62, 1042–1048.
Scheffold, F., 2002. Particle sizing with diffusing wave spectroscopy. J. Dispersion Sci. Technol. 23, 591–599.
Schmitt, O., On-line particle analysis in wet processes, Chemie. DE, 〈http://www.chemie.de/articles/e/61506〉.
Schönfeld, F., Hessel, V., Hofmann, C., 2004. An optimised split-and-recombine micro mixer with uniform 'chaotic' mixing. Lab Chip 4, 65–69.
Schwesinger, N., Frank, T., Wurmus, H., 1996. A modular microfluidic system with an integrated micromixer. J. Micromech. Microeng. 6, 99–102.
Sobolík, V., Tihon, J., Wein, O., Wichterle, K., 1998. Calibration of electrodiffusion friction probes using voltage-step transient. J. Appl. Electrochem. 28, 329–335.
Stapf, S., Han, S., 2005. NMR Imaging in Chemical Engineering. Wiley, Weinheim.
Stokes, D.J., Thiel, B.L., Donald, A.M., 1998. Direct observation of water-oil emulsion systems in the liquid state by environmental scanning electron. Microsc. Langmuir 14, 4402–4408.
Stroock, A.D., Dertinger, S.K.W., Ajdari, A., Mezic, I., Stone, H.A., Whitesides, G.M., 2002. Chaotic mixer for microchannels. Science 295, 647–651.
Sugiura, S., Nakajima, S., Iwamoto, S., Seki, M., 2001. Interfacial tension driven monodispersed droplet formation from microfabricated channel array. Langmuir 17, 5562–5566.
Thakur, R.K., Vial, Ch., Nigam, K.D.P., Nauman, E.B., Djelveh, G., 2003. Static mixers in the process industries—a review. Chem. Eng. Res. Des. 81A, 787–826.
Tice, J.D., Lyon, A.D., Ismagilov, R.F., 2004. Effects of viscosity on droplet formation and mixing in microfluidic channels. Anal. Chim. Acta 507, 73–77.
Tice, J.D., Song, H., Lyon, A.D., Ismagilov, R.F., 2003. Formation of droplets and mixing in multiphase microfluidics at low values of the Reynolds and the capillary numbers. Langmuir 19, 9127–9133.
Tihon, J., Legrand, J., Legentilhomme, P., 2001. Near-wall investigation of backward-facing step flows. Exp. Fluids 31, 484–493.
Tihon, J., Serifi, K., Argyriadi, K., Bontozoglou, V., 2006. Solitary waves on inclined films: their characteristics and the effect on wall shear stress. Exp. Fluids 41, 79–89.
Tihon, J., Tovčigrečko, V., Sobolík, V., Wein, O., 2003. Electrodiffusion detection of the near-wall flow reversal in liquid films at the regime of solitary waves. J. Appl. Electrochem. 33, 577–587.
Timgren, A., Trägardh, G., Trägardh, C., 2008. Application of the PIV technique to measurements around and inside a forming drop in a liquid–liquid system. Exp. Fluids 44, 565–575.
van Dalen, G., 2002. Determination of the water droplet size distribution of fat spreads using confocal scanning laser microscopy. J. Microsc. 208, 116–133.
van der Linden, E., Sagis, L., Venema, P., 2003. Rheo-optics and food systems. Curr. Opinion Colloid Interface Sci. 8 (4–5), 349–358.
van der Zwan, E., Schroen, K., van Dijke, K., Boom, R., 2006. Visualization of droplet break-up in pre-mix membrane emulsification using microfluidic devices. Colloids Surf. A Physicochem. Eng. Aspects 277 (1–3), 223–229.
van Steijn, V., Kreutzer, M.T., Kleijn, C.R., 2007. μ-PIV study of the formation of segmented flow in microfluidic T-junctions. Chem. Eng. Sci. 62, 7505–7514.
Waelchli, S., von Rohr, P.R., 2006. Two-phase flow characteristics in gas–liquid microreactors. Int. J. Multiphase Flow 32, 791–806.
Wang, C., Nguyen, N.-T., Wong, T.N., 2007. Optical measurement of flow field and concentration field inside a moving nanoliter droplet. Sensors Actuators A 133, 317–322.
Warnier, M.J.F., Rebrov, E.V., de Croon, M.H.J.M., Hessel, V., Schouten, J.C., 2008. Gas hold-up and liquid film thickness in Taylor flow in rectangular microchannels. Chem. Eng. J. 135S, S153–S158.
Wolffenbuttel, B.M.A., Stankiewicz, T.A., Moulijn, J.A., 2002. Novel method for non-intrusive measurement of velocity and slug length in two- and three-phase slug flow in capillaries. Meas. Sci. Technol. 13, 1540–1544.
Wong, S.H., Ward, M.C.L., Wharton, C.W., 2004. Micro T-mixer as a rapid mixing micromixer. Sensors Actuators B 100, 359–379.
Wooster, T.J., Augustin, M.A., 2006. Beta-Lactoglobulin-dextran Maillard conjugates: their effect on interfacial thickness and emulsion stability. J. Colloid Interface Sci. 303 (2), 564–572.
Wu, Z.G., Nguyen, N.T., 2005. Hydrodynamic focusing in microchannels under consideration of diffusive dispersion: theories and experiments. Sensors Actuators B 107, 965–974.
Xiong, R., Bai, M., Chung, J.N., 2007. Formation of bubbles in a simple co-flowing micro-channel. J. Micromech. Microeng. 17, 1002–1011.
Yu, Z., Heraminger, O., Fan, L.-S., 2007. Experiment and lattice Boltzmann simulation of two-phase gas–liquid flows in microchannels. Chem. Eng. Sci. 62, 7172–7183.
Yue, J., Chen, G., Yuan, Q., Luo, L., Gonthier, Y., 2007. Hydrodynamics and mass transfer characteristics in gas–liquid flow through a rectangular microchannel. Chem. Eng. Sci. 62, 2096–2108.